Investigation on combustion characteristics and emissions of biogas/hydrogen blends in gas turbine combustors

New Journal and we have not received input yet 27 (2022) 101178

Contents lists available at ScienceDirect

Thermal Science and Engineering Progress

journal homepage: www.sciencedirect.com/journal/thermal-science-and-engineering-progress

Investigation on combustion characteristics and emissions of biogas/hydrogen blends in gas turbine combustors

Sabrina Benaissa [a,*], Belkacem Adouane [a], S.M. Ali [b,c], Sherif S. Rashwan [d], Z. Aouachria [a]

[a] Department of Physics/Research Laboratory LPEA, University of Batna 1, Batna, Algeria
[b] Department of Aerospace Engineering, Indian Institute of Technology Madras, Chennai, India
[c] Department of Mechanical Engineering, Eindhoven University of Technology, Eindhoven, Netherlands
[d] Mechanical Power Department, Faculty of Engineering, Cairo University, 12613 Giza, Egypt

ARTICLE INFO

Keywords:
Biogas-hydrogen fuel
Non-premixed
Steady laminar flamelet model
Stable flame operation
Emissions
clean combustion

ABSTRACT

In the present work, numerical investigations are performed to study the combustion characteristics of biogas fuel blended with hydrogen at various compositions for a non-premixed swirling flame in a can-type gas turbine combustor. The amount of hydrogen enrichment varies from 0 to 50% by volume. A numerical approach using the non-premixed flamelet model, turbulent standard (k–ε) model, and P-1 radiation model was adopted for simulating the can-type combustor power at a fixed operating power of 60 kW. The steady laminar flamelet model was used to analyze the effect of hydrogen enrichment, global equivalence ratio with different swirl numbers on a stable flame operation, temperature distribution and contours, velocity streamline contours, NO emissions, and species concentrations. The results indicate that hydrogen enrichment and the variation of the equivalence ratio and the swirl numbers significantly impacted the flame macrostructure. Hydrogen enrichment in the fuel intensifi combustion, leading to higher flame temperature and wider flammability than bure biogas. Maximum NO emissions in the outlet chamber have been dropped by 43 and 78 (ppm @15 % by volume of O_2) for the biogas and biogas-50% H_2, respectively, due to the reduced flame temperature leading to reduction in thermal NOx formation with reduction equivalence ratio from 0.5 to 0.2. The flame temperature and NO emissions at $\phi = 0.2$ with a high rate of hydrogen (50% H_2) are close to the results of pure biogas (0% H_2) at the same equivalence ratio. The results show that CO and CO_2 emissions decrease with increasing hydrogen addition and decreasing the equivalence ratio; due to a decrease in the amount of carbon, the cooling effect, and an increase in the OH concentration.

Introduction

Due to growing energy demand leading to climate change, the general strategy is to reduce dependency on fossil fuels consumption (e.g., natural gas, petroleum, coal) and search for alternate green fuel options [1,2]. Thus, understanding the applicability of alternative green fuels and their combustion/oxidation characteristics in the existing Internal Combustion engines (ICEs) and gas turbine engines (GTs) has received significant attention worldwide in recent decades. Biogas is a promising substitute among these alternative green fuels due to its lower processing cost and slightly higher density than natural gas. Biogas is a renewable gaseous fuel that will likely play a pivotal role in protecting the environment due to reduced combustion emissions [3]. Biogas production is operated on both micro or industrial scales. Biogas is produced from the anaerobic degradation of organic waste and mainly contains methane and carbon dioxide (generally 60% CH_4 and 40% CO_2). Its physical properties are comparable to natural gas, which is 99% CH_4. Biogas can also be transported easily due to similar physical properties as natural gas [4]. However, the calorific value of biogas is low compared to other conventional fuels. For instance, at 1 atm and 15 °C, the lower heating value (LHV) of biogas (57% CH_4, 41% CO_2 and traces of other gases) is around 1/3 (17 MJ./kg) of natural gas (50 MJ/kg) and 1/1 hydrogen (120 MJ/kg), respectively [5,6]. Therefore, the usage of 100% biogas as fuel in the burners (CI engines or gas turbines) is limited by the potential flame stability, narrow flame stability flammability limit, low-temperature flames, and low burning velocities. It is undoubtedly beneficial if the biogas is mixed with hydrogen because hydrogen has favorable combustible properties such as high reactivity, very low ignition delay, high flame speed, higher combustion density,

* Corresponding author.
E-mail addresses: Sabrina.benaissa@univ-batna.dz (S. Benaissa), smughees.ali@gmail.com (S.M. Ali).

https://doi.org/10.1016/j.tsep.2021.101178
Received 18 June 2021; Received in revised form 22 October 2021; Accepted 14 December 2021
Available online 18 December 2021

Nomenclature

C	linear-anisotropic phase function coefficient
Cp	specific heat (J/kg-K)
$C1\varepsilon$, $C2\varepsilon$, $C\mu$	constants in turbulence model equations
D	mass diffusivity of species
E	total energy (kJ/kg)
f	mixture fraction (dimensionless)
$\tilde{f}$	mean mixture fraction
f''	mixture fraction variance
G	the medium refractive index (dimensionless)
HHV	higher heating value (M.J./m^3)
k	turbulent kinetic energy (m^2/s^2)
k	thermal conductivity (W/m.K)
LHV	lower heating value (M.J./m^3)
$\dot{m}$	mass flow rate (kg/s)
n	the medium refractive index (dimensionless)
P	burner power (MW)
p	pressure (Pa)
P_{rt}	turbulent Prandtl number (dimensionless)
P_k	the production of the turbulence kinetic energy kg/ms^3)
Q	volume flows (m^3/s)
q_r	radiation flux (W/m^2)
R	outer radius of the annulus (m
Re	Reynolds number (dimensionless)
R_H	hydrogen fraction in the fuel
S_G	user-defined radiation source
S_h	term source includes the heat of chemical reactions, radiation and any other volumetric heat sources
SN	Swirl number (dimensionless)
T	Temperature (K)
u, v, w	velocity magnitude (m/s)
WI	Wobbe Index (M.J./m^3)
Z	the elemental mass fraction for element 'i' (dimensionless)

Greek letters

a	absorption coefficient (m^{-1})
α	molar fraction of carbon dioxide (dimensionless)
β	various minimum oxygen requirements of the fuel species (dimensionless)
γ	mole fraction of the hydrogen (dimensionless)
ξ	hydrogen mole fraction of products (dimensionless)
δ	delta function (units vary)
ρ	density (kg/m^3)
υ	the kinematic viscosity (m^2/s)
μ	dynamic viscosity (kg/m-s)
μ_t	the turbulent viscosity (kg/m-s)
τ	stress tensor (Pa)
ε	dissipation of the turbulent kinetic energy (m^2/s^3)
ϕ	global equivalence ratio (dimensionless)
σ	constant of Stefan-Boltzmann(5.67 $\times$ 10^{-8} W/m^2-K^4)
σ_k	the turbulent Prandtl numbers for k
σ_ε	the turbulent Prandtl numbers for ε.
σ_s	the scattering coefficient (m^{-1})

and lower CO_2 emissions [7,8]. It is known that the utilization of 100% hydrogen in IC engines or gas turbines has numerous problems related to safety, storage and economics of scales [9]. To overcome these issues, many researchers have proposed adding hydrogen to alternative fuels. The recent work of Benaissa et al. [10] has shown that adding 10 to 50 % of hydrogen in the biogas (60% CH_4/40% CO_2) fuel improves ignition delay (5 to 10 times) and laminar flame speed (2 to 3 times). This study has also developed the laminar flame speed analytical correlations for biogas/hydrogen-air mixtures relevant for IC engines and gas turbine combustor operating conditions. Several studies from the past have investigated experimentally and numerically the impact of hydrogen additions to fuels in internal combustion engines (ICs) and gas turbines (GTs), as presented in Table 1. According to these studies, using hydrogen as fuel in ICs and GTs improves the combustion characteristics, such as reducing NOx emissions and high-speed engine operation. The higher flame speed and wider flammability limit allow lean to ultra-lean operation, enabling lower NOx emissions, higher efficiency and output power.

The hydrogen enrichment to hydrocarbon-air mixtures enhances combustion intensity, primarily by extending the flammability limits for lean mixtures, which are the key characteristics of the fuel mixture to use in gas turbines the internal combustion engines. Wei et al. [17] have experimentally studied the effects of unburned gas velocity on the CO and NOx formations rate of the laminar premixed biogas-hydrogen mixtures. The results illustrate that the flame at a higher Reynolds Number (Re) can improve the ambient air mixing in the diffusion-combustion zone. CO oxidation can be improved by a more significant flow rate and higher flow velocity. Zhen et al. [18] investigated the stability and thermal emission characteristics of biogas-H_2-air premixed flames using a Bunsen burner. They reported that the laminar flame speed of biogas-air mixtures increases monotonically with H_2 addition. These results are also confirmed in the recent study of Benaissa et al. [10] and further used to develop the analytical laminar flame speed correlations.

Hydrogen can also be obtained from a renewable source, such as syngas, which contains a significant amount of hydrogen. Upgrading syngas to hydrogen and mixing it with biogas gives a good alternative for fossil fuels. It can be produced on industrial scales and supplied to installations or engines. Furthermore, improved stable flame operation and reduced emission are associated with hydrogen addition. Ali and Varunkumar [19,20] have performed experimental and computational extinction strain rate studies for methane-air and syngas-air non-premixed flames using an extensive range of CO/H_2 ratios of 1 to 49. Ali and Varunkumar [19] have developed a three-step global kinetic model for syngas non-premixed flames to predict extinction relevant for combustors. These studies show that the extinction strain rate increases by 2 to 3 times by increasing only 4% H_2 in the fuel mixture leading to significant improvement in the overall mixture reactivity [19,20]. Wei et al. [21] performed a numerical analysis of the one-dimensional laminar premixed flames of H_2 enriched biogas-air using a detailed GRI mech 3.0 reaction kinetics mechanism. They found that the global heat release rate decreases as CO_2 is introduced due to combined thermal and chemical effects. They observed that the addition of H_2 to the biogas-air significantly enhance the global heat release rates. Mameri and Tabet [22] studied the effect of several operating conditions on the flame structure and NO emissions of a biogas-hydrogen enrichment diffusion flame numerically. The results illustrate that the biogas-H_2 mixture increases the value of the heating mixture and leads to enhanced fuel reactivity. This is due to the increase in the concentration of H, OH, and O radicals. Benaissa et al. [10] have shown a 1.5 to 2 times increase in H and OH radical peaks with 50 % addition of H_2 in the biogas for laminar premixed flames for a wide range of equivalence ratios (0.7–1.4) and initial conditions (initial pressure and temperature of 0.1–7 Mpa and 300–600 K, respectively).

Despite the benefits of hydrogen enrichment in biogas fuel, limited studies have been found in the literature, especially for gas turbine applications. Research studies have presented several important parameters that influence combustion instability characteristics in gas turbines:

Table 1
Impact of hydrogen additions to fuels in internal combustion engines (ICs) and gas turbines (GTs).

Year	Authors	Application	Type of study	Findings
2008	C D Rakopoulos et al. [11]	Spark ignition (SI) engine	Experimental study	Hydrogen enrichment in biogas can increase the second-law efficiency of engine operation (from 40.85 % to 42.41%) by reducing the combustion-generated irreversibility (from 18.25 % to 17.18 %). The increases in H_2 addition in biogas led to increased combustion temperatures and decreased combustion duration, thus reducing the combustion irreversibility.
2006	GL Juste et al. [12]	Industrial gas turbine combustor	Experimental study	By injecting small amounts of hydrogen-air mixture into the lean primary zone, it is possible to reduce the level of nitrogen oxides (NOx).
2010	K.K. Gupta et al. [13]			Increasing the primary air in gas turbine combustor is an effective way to reduce NOx emissions, but at a lower efficiency cost because carbon dioxide and hydrocarbons emissions increase.
1997	Noriyuki Kobayashi et al. [14]	Gas-turbine system	Experimental study	The effects of equivalence ratio and swirl number in gas turbines were studied, and the NOx emission is highly dependent on the swirl number and the equivalence ratio. Swirl was effective in reducing the emission of nitrogen oxides.
2014	A. Aziz Hairuddin et al. [15]	Diesel compression ignition engines	Review experimental study and Numerical methods	Hydrogen addition becomes a natural choice to improve diesel engine performance and emissions.
2015	Hayder A. Alrazen et al. [16]			Hydrogen addition would affect emissions; as a decrease in non-combustible hydrocarbons, carbon dioxide (CO_2), carbon monoxide (CO), and particulate matter (PM) emissions, there is also an increase in the (NOx) when enriching H_2. However, it can be controlled by exhaust gas recirculation (EGR) and by controlled injections.

the swirl number, equivalence ratio, combustion design, and fuel compositions. Jalalatian et al. [23] have performed experiments on the effect of the swirl number, equivalence ratio, and Reynolds numbers on diffusion flame structure and pollutant emissions. They demonstrated that when the overall equivalence ratio (the global equivalence ratio) increases, the flame length enhances, increase in swirl number leads to a slight decrease in temperature, CO concentrations, and NO thermal concentrations. Kotb and Saad [24] have predicted the effect of equivalence ratio on the flame stability and CO concentration. As a result, the swirl burner displays a lower CO concentration than the co-flow burner. Yılmaz [25] has performed experiments on the Swirl Number effect on the combustion characteristics of natural gas diffusion flames and has been validated and compared with a simulation using a standard k-epsilon model. He proved that the swirl number strongly affects combustion characteristics like the flame temperature, the gas CH_4, CO_2, O_2, and H_2O concentrations.

The most commonly used combustion model is the steady laminar flamelet (SLF) model presented by Peters [26]. It is observed that the GRI (detailed chemical reaction mechanism: mech 3.0) is a popular choice for simulating the SLF model for biogas-hydrogen combustion and has been widely chosen for the biogas-hydrogen combustion mixture [27–29] successfully in the past. GRI mech 3.0 contains 53 species and 325 reactions. Most importantly, it contains the constituent elements of biogas interactions (C_1-C_3), including a detailed combustion H_2 mechanism. Some research studies reported biogas combustion characteristics as fuel, but mostly they are concerned about internal combustion engines [30]. However, knowledge of the combustion characteristics of hydrogen-enriched biogas combustion in gas turbine combustors is undoubtedly insufficient for describing the best-operating conditions in terms of equivalence ratio and the corresponding exhaust gas emissions, namely, NOx, CO, and CO_2. The present study attempts to predict the possible combustion characteristics of biogas-hydrogen blends to provide a vital aspect of the static stability in a can-type combustor. The challenge is simultaneously solving different models, including the reacting flow, combustion module, and turbulence model.

The present study's motivation is to get insights into the flame stabilization inside the gas turbine combustor. Therefore, in the current work, the hydrogen/biogas flames are simulated inside the can-type combustor is to study the effect of the hydrogen enrichment and the variation of equivalence ratio and swirl numbers on the flame stabilization, emissions and to reach the optimum operability condition. The improvement of biogas combustion properties is by hydrogen enrichment; however, this increases the flame temperature and NOx emissions. In order to get rid of this defect, the optimum range of hydrogen and equivalence ratio has been studied and presented in this work.

Numerical modeling

Numerical computations were performed for the hydrogen/biogas flame inside the can-type combustor. In this study, we have selected four global equivalence ratios ($0.2 \leq \phi \leq 0.5$) to be investigated. For better

clarification, each equivalence ratio has six simulations (biogas doped with (0% to 50%) hydrogen), full simulations for four equivalence ratios are 24, all simulations were performed under a constant burner power of 60 kW in a can-type combustor. A detailed description of the computational domain, governing equations, representative chemical and physical properties, boundary conditions and meshing and solver details used for 3D computations are given below.

Computational domain

The schematic of the three-dimensional computational domain of the can-type combustion chamber is shown in Fig. 1. The dimensions of the combustor chamber are (Z ~ 0.59 m, Y ~ 0.25 m, X ~ 0.23 m). The primary air is directed through the vanes to supply the air with a swirling velocity. The diameter of the primary air hole is 0.10 m with a vane angle of 45°. The swirl numbers (refer to Eqn. (26) for details) larger than 0.7 are typically used in a can-type combustor, creating a vortex reverse flow. The swirl (SN) and Reynolds (Re) numbers used in the current study are provided in Table 2. The fuel and the secondary air were injected through the six holes. The secondary air was injected at 0.1 m from the fuel injector. The diameter of the fuel and the secondary air of holes is 0.0042 m and 0.0016 m, respectively.

Fuel and air were injected separately, creating a non-premixed flame. The outlet has a surface area rectangular form of 0.015 m^2.

Governing equations

The governing equations for a steady turbulent non-premixed combustion (continuity, momentum, energy, and additional equations for the standard k-ε turbulence model, radiation, and combustion) solved for the current study are shown below [31–34].

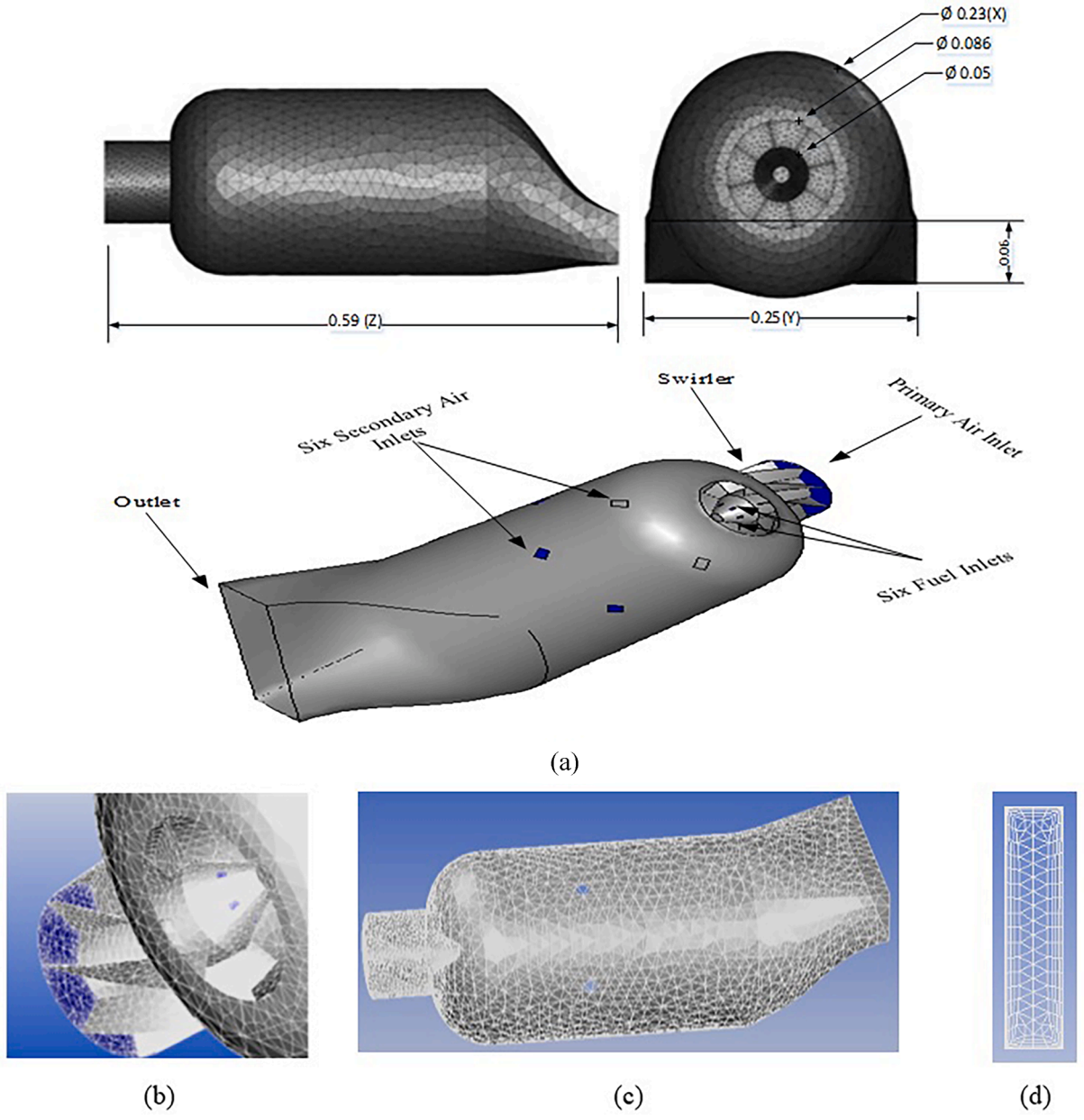

Fig. 1. Three-dimensional can-type computational domain of combustion chamber with the mesh, (a) Combustion chamber details with dimensions, (b) air–fuel inlet, (c) combustor chamber, (d) combustor chamber outlet.

Table 2
Can-type gas turbine operational conditions with fuels compositions at 300 K atmospheric pressure.

ϕ	Swirl number (SN)	Reynolds (Re)	P (KW)	Fuel Mass flow (kg /s)	Air Mass flow (kg / s)
0.5	0.77–0.73	25810–24354	60	3.4×10^{-3}-2.4×10^{-3}	$4.1 \times 10^{-2} - 3.88 \times 10^{-2}$
0.4	0.89–0.84	32626–30774	60	3.4×10^{-3}-2.4×10^{-3}	$5.13 \times 10^{-2} - 4.85 \times 10^{-2}$
0.3	1.03–098	43943–41429	60	3.4×10^{-3}-2.4×10^{-3}	$6.84 \times 10^{-2} - 6.46 \times 10^{-2}$
0.2	1.22–1.18	66842–62805	60	3.4×10^{-3}-2.4×10^{-3}	$1.03 \times 10^{-1} - 9.69 \times 10^{-2}$

Fuel compositions (vol. %)			Air compositions (vol. %)		Fuel Densityg·m^{-3}	Fuel HHVMJ·m^{-3}	Fuel LHVMJ·m^{-3}	Fuel Specific Gravity	Wobbe IndexMJ·m^{-3}
CH_4	CO_2	H_2	O_2	N_2					
60	40	0	21	79	1219.564	23.933	21.568	0.943	24.641
54	36	10	21	79	1105.772	22.802	20.478	0.855	24.655
48	32	20	21	79	992.244	21.675	19.392	0.768	24.740
42	28	30	21	79	878.951	20.551	18.309	0.680	24.923
36	24	40	21	79	765.862	19.430	17.228	0.592	25.244
30	20	50	21	79	652.947	18.312	16.150	0.505	25.766

Continuity equation

$$\frac{\partial \overline{\rho}\widetilde{u}_i}{\partial x_i} = 0 \tag{2}$$

Momentum equation

$$\frac{\partial \overline{\rho} u_i u_j}{\partial x_i} = -\frac{\partial \overline{p}}{\partial x_j} + \frac{\partial}{\partial x_i}\left(\overline{\tau_{ij}} - \overline{\rho} u''_i u''_j\right) \tag{3}$$

The Reynolds stresses $\overline{\rho}(u_i'' u_j'')$ are determined using Boussinesq expression.

$$\overline{\rho} u''_i u''_j = -\mu_t\left(\frac{\partial u_i}{\partial x_j} + \frac{\partial u_j}{\partial x_i} - \frac{2}{3}\delta_{ij}\frac{\partial u_k}{\partial x_k}\right) + \frac{2}{3}\overline{\rho} k \tag{4}$$

Where μ_t is a turbulent dynamic viscosity calculated using Eqn. (7), with τ_{ij} is the viscous tensor.

$$\tau_{ij} = \mu\left(\left(\frac{\partial u_i}{\partial x_j} + \frac{\partial u_j}{\partial x_i}\right) - \frac{2}{3}\delta_{ij}\frac{\partial u_k}{\partial x_k}\right) \tag{5}$$

It was added the last term in Eqn. (3) to restore the correct expression of the turbulent kinetic energy k.

$$k = \frac{1}{2}\sum_{k=1}^{3} u''_k u''_k \tag{6}$$

The turbulent kinetic energy (k) equation is given as follows.

$$\frac{\partial\left(\overline{\rho}\widetilde{u}_i k\right)}{\partial x_i} = \frac{\partial[(\mu + \mu_t/\sigma_k)(\partial k/\partial x_i)]}{\partial x_i} + P_k - \overline{\rho}\varepsilon \tag{7}$$

where

$$\mu_t = \overline{\rho} C_\mu \frac{k^2}{\varepsilon} \tag{8}$$

$C\mu = 0.99$ is constant, σ_k is the turbulent Prandtl numbers for k. Also, $\sigma_k = 1$ and P_k is the production of the turbulence kinetic energy, due to the mean velocity gradients, it defined as-

$$P_k = -\overline{\rho}\widetilde{u''_i u''_j}\frac{\partial \widetilde{u}_i}{\partial x_j} \tag{9}$$

The dissipation kinetic energy (ε) equation is as follows.

$$\frac{\partial\left(\overline{\rho}\widetilde{u}_i \varepsilon\right)}{\partial x_i} = \frac{\partial[(\mu + \mu_t/\sigma_\varepsilon)(\partial \varepsilon/\partial x_i)]}{\partial x_i} + C_{\varepsilon 1}\frac{\varepsilon}{k}P_k - C_{\varepsilon 2}\overline{\rho}\frac{\varepsilon^2}{k} \tag{10}$$

where $C_{\varepsilon 1} = 1.44$, $C_{\varepsilon 2} = 1.92$ and $\sigma_\varepsilon = 1.3$ where σ_ε is the turbulent Prandtl numbers for ε.

The energy equation is given as follows [31,35–37].

$$\frac{\partial}{\partial x_i}\left(\widetilde{u}_i\left(\rho\widetilde{E} + \overline{p}\right)\right) = \frac{\partial}{\partial x_j}\left(\left(k + \frac{c_p u_t}{Pr_t}\right)\right)\frac{\partial \widetilde{T}}{\partial x_j} + \widetilde{u}_i\left(\overline{\tau_{ij}}\right)_{eff} + S_h \tag{11}$$

where k presents thermal conductivity, Pr_t is the turbulent Prandtl number, S_h is the term source that includes the heat of chemical reaction, radiation, and any other volumetric heat sources. E represents the total energy in Eqn. (10). Here, $(\tau_{ij})_{eff}$ is the deviator stress tensor (the viscous heating) given as follows.

$$\left(\tau_{ij}\right)_{eff} = \mu_{eff}\left(\left(\frac{\partial u_i}{\partial x_j} + \frac{\partial u_j}{\partial x_i}\right) - \frac{2}{3}\delta_{ij}\frac{\partial u_i}{\partial x_i}\right) \tag{12}$$

The radiation flux equation (q_r) [31,38,39].

$$q_r = -\frac{1}{3(\alpha + \sigma_s) - C_{\sigma_s}}\nabla G \tag{13}$$

where a, σ_s and C are the absorption, the scattering coefficients, and the linear-anisotropic phase function coefficient, the G is the incident radiation.

(13) The transport equation for G is given below.

$$\nabla.(\Gamma \nabla G) - a G + 4\, a\, n^2 \sigma T^4 = S_G \tag{14}$$

where, n is the medium refractive index, σ is the constant of Stefan-Boltzmann, and S_G is a user-defined radiation source. Here,

$$\Gamma = -\frac{1}{3(\alpha + \sigma_s) - C_{\sigma_s}} \tag{15}$$

When the P-1 model is active, this transport equation (Eqn. (13)) calculates the local incident radiation. Reaction rates are related using the mixture fraction (f) equation.

Mixture fraction (*f*)

$$\frac{\partial}{\partial x_i}\left(\overline{\rho}u_i f\right) = \frac{\partial}{\partial x_i}\left(\overline{\rho D\frac{\partial f}{\partial x_i}} - \overline{\rho}u''_i f''\right) \tag{16}$$

where

$$f = \frac{Z_i - Z_{i,ox}}{Z_{i,fuel} + Z_{i,ox}} \tag{17}$$

where $\overline{D}$ is a "mean" species molecular diffusion coefficient, Z is the elemental mass fraction for element i. the indices ox, fuel present the oxidizer/fuel stream inlets values. Pre-generated flamelet table (or a lookup table) in terms of mixture fraction (*f*) and scalar dissipation rate were used to model chemistry. Beta-shaped PDF in terms of mixture fraction and scalar dissipation was used for turbulent-chemistry closure, and two addition transport equations of are mixture fraction (*f*) and its variance ($\overline{f''^2}$) were solved.

Chemical reaction & other physical properties

The chemical composition is calculated using the air/fuel stoichiometric and the mass flow of air/fuel, the adiabatic temperature, the burner power for the biogas, and biogas-enhanced and the following reactions. First is the overall chemical reaction of biogas given as-

$$(1-\alpha)[CH_4 + \beta\ (O_2 + 3.76N_2)] + \alpha\, CO_2 \rightarrow CO_2 + 2(1-\alpha)\ H_2\ O + \beta\ (1-\alpha)N_2 \tag{18}$$

β: the various minimum oxygen requirements of the fuel species, α: the molar fraction of carbon dioxide, for a global equivalence ratio $\phi = 1$, $\alpha = 0.4$:

$$0.6\ \ CH_4 + 1.2(O_2 + 3.76\ \ N_2) + 0.4\ \ CO_2 \rightarrow CO_2 + 1.2\ \ H_2O + 4.512\ \ N_2 \tag{19}$$

The chemical reaction of biogas/hydrogen blends (at the stoichiometric) is given as-

$$(1-\gamma)[(1-\alpha)\ \ CH_4 + \alpha\, CO_2] + \gamma H_2 + \beta(O_2 + 3.76\ \ N_2) \rightarrow (1-\gamma)\, CO_2 + \ \xi H_2O + 3.76\beta\, N_2 \tag{20}$$

where γ: the mole fraction of the hydrogen, ξ: the hydrogen mole fraction of products, for example, the stoichiometric combustion equation, for fuel consisting in a volume of 54% methane, 10% hydrogen and 36% carbon dioxide:

$$(0.54\ CH_4 + 0.36\ CO_2) + 0.1\ H_2 + 1.13\ (O_2 + 3.76\ N_2) \rightarrow 0.9\ CO_2 + 1.18\ H_2O + 4.2488\ N_2 \tag{21}$$

One of the properties that are very important in combustion is the equivalence ratio [40], which is the normalizing of the actual fuel–air ratio by the stoichiometric fuel–air ratio:

$$\phi = \frac{Actual\ F/A\quad ratio}{Stoichiometric\ F/A\ ratio} \tag{22}$$

There are three types of flames (mixture), ϕ greater than 1 is a rich mixture, $\phi = 1$ is a stoichiometric mixture, and ϕ less than 1 is a lean mixture, in our case $0.2 \leq \phi \leq 0.5$ (excess of air), which is the standard practice for combustion in gas turbines.

The calculations are made by vol. %, since the biogas is commonly measured by Gas Chromatography [41] (GC) in vol.%. Also, most of the literature references have used vol. % for fuel and oxidizer flowrate. The stoichiometric fuel to oxidizer is calculated by the oxygen required for the mixture.

$$stoichiometric\ A/F = ((2 \times CH_4\%) + (0.5 \times H_2\%))/0.21 \tag{23}$$

In this work, all the comparisons for the biogas and biogas-H_2 blends are performed at a fixed overall equivalence ratio. The equation of flame power (MW) is used to infer the volume flows (Q in (m^3/s)):

$$P(MW) = LHV_{biogas} \times Q_{biogas} + LHV_{H_2} \times Q_{H_2} \tag{24}$$

All the computations are performed at fixed combustor power of 0.06 MW or 60 kW. The lower heating value of the fuel (biogas doped by H_2 %) is calculated using Eqn. (24).

$$LHV(Fuel) = (CH_4\%{*}LHV_{CH_4}) + (H_2\%{*}LHV_{H_2}) \tag{25}$$

With the $LHV_{CH4} = 35.87$ (MJ/m^3), and $LHV_{H2} = 10.75$ (MJ/m^3), respectively.

Fuel and air mass flow rates were calculated (Eqn. (25)) by multiplying their densities (ρ) with their respective volume flow rates (*Q*).

$$\dot{m} = \rho \times Q \tag{26}$$

The swirl number (SN) is defined as a dimensionless parameter; the ratio of the tangential momentum flux over the axial momentum flux is used to study the effect of the airflow swirling inlet on the flame combustion characteristics [42].

$$S = G_{tg}/RG_{ax} = \int_0^R \rho u w r^2\, dr \Big/ R\int_0^R \rho u^2 r\, dr \tag{27}$$

In the Eqn. (26), G_{tg} and G_{ax} represent the axial flux of the tangential momentum and the axial flux of the axial momentum, respectively. *R* is the outer radius of the annulus, *u*, and *w* are the axial velocity and tangential at the radial position *r*, respectively. The Wobbe index (WI) is a standard indicator of gas turbines' fuel characteristics and interchangeability, counting power facilities and original equipment manufacturers (OEMs). It was developed to describe the fuel gas with different compositions [43].

$$WI = \frac{HHV_{fuel,Vol}}{\sqrt{\rho_{fuel}/\rho_{air}}} \qquad MWI = \frac{LHV_{fuel,Vol}}{\sqrt{T_{gas}\,\rho_{fuel}/\rho_{air}}} \tag{28}$$

WI is presented as the fuel higher heating value (HHV) in our case is a gas divided by the ratio of fuel density to air density. The Modified Wobbe Index (MWI) contains the lower heating value (LHV) and the fuel temperature.

Boundary conditions, solver details

The operating conditions of the fuel and airflow inlets are summarized in Table 2. The fuel and airflow inlets were temperature maintained at 300 K, and all the simulations were performed at atmospheric pressure with a turbulence intensity of 10%. The fuel mass flow varies by LHV due to the change in fuel compositions, and the air mass flow was varied with a global equivalence ratio range (0.5 to 0.2) such that combustor power was equal to 60 KW. The hydrogen fraction in the biogas fuel (60% CH_4 and 40% CO_2) was varied from 10 to 50% (v/v). The secondary air was injected with a mass flow rate of 0.002 kg/s at a temperature equal to 300 K with a turbulence intensity of 10%.

The standard k-ε turbulence model was used for simulations, and its choice is justified from the past studies. Several studies have used the Reynolds-averaged Navier Stokes (RANS) approach with the standard k-epsilon model for swirling flow. Marzouk and Huckaby [44] performed several numerical simulations of swirling airflow using three versions of the k-ε turbulence model (standard, realizable, and renormalization group RNG); They have compared their result with experimental mean velocity profiles. Their results showed that the standard model (SKE) achieved the best overall performance. In contrast, the realizable model was unable to predict the radial velocity satisfactorily. It is also the most expensive model, unlike the (SKE) model. Norwazan and Mohd Jaafar [45] have focused on the effects of flow axial and tangential velocities to obtain the centre recirculation zone. The Reynolds-averaged Navier Stokes (RANS) of various models approached with standard k-ε, realizable k-ε, and RNG k-ε turbulence was applied in this study. As a result, based on the global performance of the RANS models, it appears that the standard k-ε turbulence model gives more favourable results due to the centre recirculation zone being well presented and reasonably priced, it is broader and shorter than others. This model is more economical and time-saving.

The present study is applied to model combustion with the steady laminar flamelet model (SLF). The flamelet model uses dissipation to account for deviations from equilibrium. The steady diffusion flamelet was used in the GRI mech 3.0 for modelling the combustion with 53 species and 325 reactions[46]. The scalar dissipation rate used starts from 0.01 (1/s) till extinction, and the maximum number of grid points in flamelet was taken to be equal to 64. Convergence values were step-up of the residuals where convergence criteria are 10^{-3} for all the equations except the energy and radiation equations, which we consider this criterion is 10^{-6}.The Radiation Model (P-1) was used in this simulation.

Grid independence study

A grid independence study was conducted for the 3D computations using three different meshes of sizes, 31500, 56250, and 91,900 nodes, respectively. Fig. 2(a), 2(b), 2(c), 2(d), 2(e), 2(f) and 2(g) show the comparison of mean static temperature, NO, CO_2, and CO emissions, CH_4, H_2O, and H_2 mole fractions, respectively (refer to Fig. 5 for details on the calculation of means values in the manuscript). The results demonstrate that there is no significant difference between the three meshes.

The difference is the peak values for mean static temperature, NO, CO_2, and CO emissions, CH_4, H_2O, and H_2 mole fractions is 10 K, 3.49 ppm, 0.18 %, 0.012 %, 0.0058 %, 0.2276 %, 0.00707 %, respectively. Thus, the mesh with 31 k nodes was chosen in this work to save computing power and time. Table 3 shows the details of the selected 31 k nodes mesh. For this mesh maximum cell squish is 0.94, maximum cell skewness is 0.99, and a maximum aspect ratio is 83.17, respectively.

Ghenai [47] also generated a similar mesh with similar number of nodes and the current results are validated against his published results in the subsequent section.

Results and discussion

The results related to computational validation, flame temperature, NOx, CO, CO_2 emissions on the effect of the hydrogen enrichment and the variation of equivalence ratio and swirl numbers on the stable flame operation are presented in this section. The optimal condition on hydrogen enrichment in terms of acceptable NO emissions for gas turbine operation is suggested.

Computation validation

The can-type combustor (Siemens SGT-750) has been utilized for many experimental fundamental and numerical investigations using conventional fuel and air mixtures [48–53]. Andersson et al. [54] tested the Siemens gas turbine SGT-600 and SGT-700 combustors with natural gas for Wobbe Index (WI) ranging from 25 to 55 MJ/Nm^3. In this study, the biogas-H_2 mixture fuel used has the Wobbe index of 25 M.J./Nm^3 similar to the natural gas. Additionally, according to the literature, the standard k-ε model for the Can-type combustor geometry was chosen to validate with available data in research by Ghenai et al. [47,55,56], where the natural gas (NG) is as fuel. The specific boundary conditions used to validate our model can be found in Table 4 below:

Fig. 3 displays the static temperature distribution of the natural gas composition with the same operating conditions by Ghenai et al.[55].

It is observed that the maximum temperature for natural gas equals 2110 K. It can also be seen from the results of NG, two different peaks, the first peak in the zone of the injector with the temperature equal 1810 K and the other peak in the secondary zone with the maximum temperature equal 2110 K. Also, a decrease in the temperature after primary zone Z = 0.1 m because of the air dilution. When this result was compared with the work done by Ghenai et al. [55], it was found that the present data result is in excellent agreement with their results. The average error percentage (%) is 2.79%. The following section compares flame temperature and NO emissions contours for pure biogas and biogas-hydrogen blends to quantify the effect of hydrogen addition on overall combustor performance.

Flame temperature and NO emissions contours

Fig. 4 presents the contours of the flame temperature distribution and NO emissions, with the increasing % H_2 content in the fuel for a constant equivalence ratio ($\phi = 0.5$).

These figures show that hydrogen helps maintain stable flame operation and that the flame spreads along with the combustor chamber without touching the chamber wall due to the second air dilution effect. The combustion's hot zone moves towards the central axis and expands downstream, as shown in Fig. 4 (biogas doped with 50% H_2). This indicates improved reactivity and intensifies the combustion process due to the addition of hydrogen. This is due to the combination of flow speed, flow swirl, and enhanced flame speed due to hydrogen addition and since hydrogen is 5 to 6 times more reactive than methane, thus intensifying combustion leading temperature (refer to Ali and Varunkumar [19,20] results for more details). This increase in combustion intensity can be explained by an increase in radicals (H, OH and O) concentration that accompanies a percentage increase in H_2 fraction in the fuel (refer to Benaissa et al. [10] for more details). In other words, increasing the overall reactivity will create a robust flame stable enough to resist flame extinction. This effect leads to stabile flame at a much higher strain rate without extinguishing [19,20]. Besides, it will enhance premixing between the combustible gases and incoming mixtures, which help maintain recirculation zones that promote flame stability, thus enhancing the combustion rate. It can also be seen that there is no significant change in flame temperature distribution is almost the same for a constant ϕ and burner power. Still, the NO emissions are increasing with the increase in the hydrogen rate.

Fig. 5 represents the cross-sections of flame temperature distribution

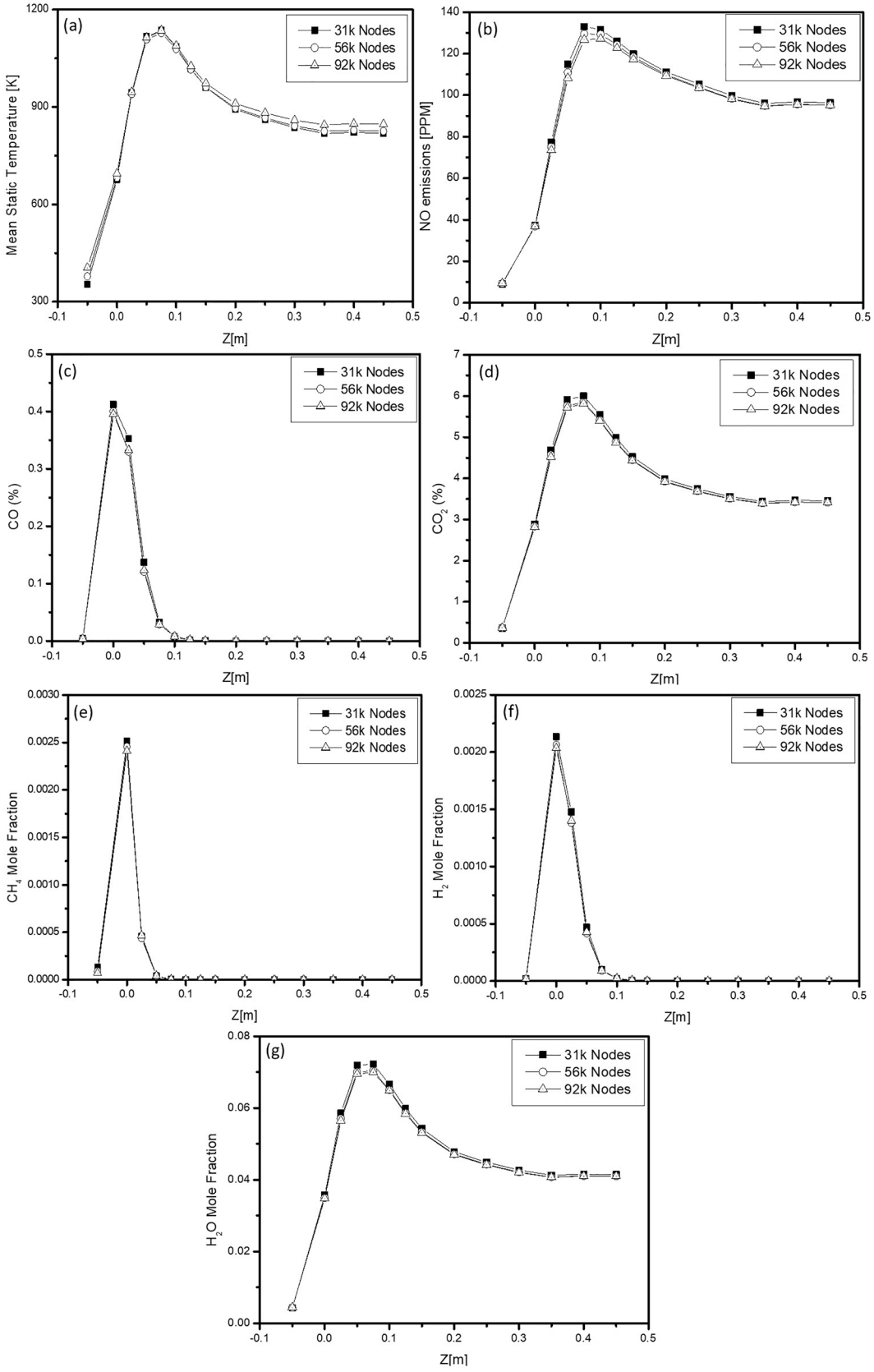

Fig. 2. Grid independence study for three different mesh sizes along axial direction; (a) mean temperature profile, (b) mean NO emissions profile, (c) mean CO_2 mole fraction profile, (d) mean CO mole fraction profile, (e) mean CH_4 mole fraction profile, (f) mean H_2O mole fraction profile, and (g) mean H_2 mole fraction profile.

Table 3
Mesh statistics.

Cell count (Number of Elements) :	106,651
1- Number of Nodes	31,433
2- Tetrahedral	74,189
3- Wedges	30,473
4- Pyramids	1989
Face count	234,368
Number of Nodes	31,433

Table 4
The detail conditions (fuel, boundary, and operating conditions)

Fuel (compositions)	Natural Gas (95%CH_4 – 0%CO_2 – 2%N_2 – 3%C_2H_6)
LHV (MJ/kg)	50
Fuel mass flow rate (kg/s)	1.0×10^{-3}
The primary air (m/s)	10
The secondary air (m/s)	6
Inlet temperature (fuel/ primary, secondary air) (K)	300
Pressure	Atmospheric pressure
Turbulence intensity	10%
Power (kW)	50

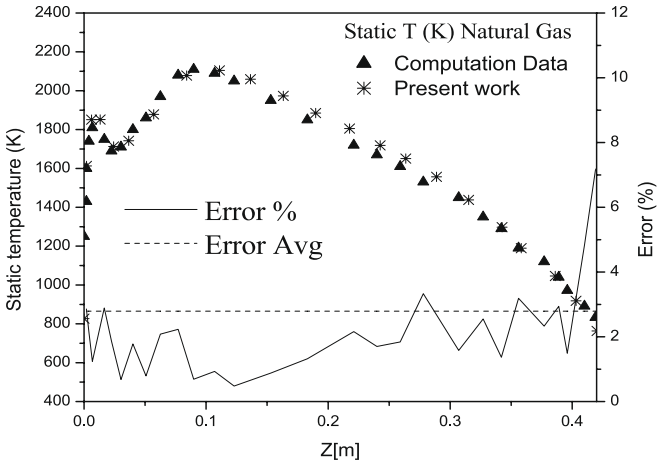

Fig. 3. Validation of the static temperature profiles of Natural gas compared to the work done by Ghenai et al.

for the biogas added with 50% H_2, at the equivalence ratio equal 0.2. This figure explains the cross-sections used to derive the results (by using surface integrals "area-weighted average"), and it starts from the fuel inlet section at Z = -0.05 m to the outlet section of the combustion chamber at Z = 0.45 m, with secondary air inlets at Z = 0.1 m.

Fig. 6 presents the contours of the flame temperature distribution and NO emission for the biogas doped with 40% H_2 for different equivalence ratios (ϕ).

The data shows that the length and thickness of the flame increase with an increase in equivalence ratio and decreases with an increase in the swirl number. Increasing swirl number leads to reduced available reaction time between the oxygen and nitrogen molecules in the hot zone (reaction region); ultimately, it reduces nitrogen oxides production. For that, the NOx exhaust decreases.

Despite the large proportion of air for the equivalence ratio equal to 0.2, the flame is not extinguished with these chosen new boundary conditions. The length and thickness of NO emissions decreased because of the decrease in the temperature and the equivalent between the air primary/secondary and fuel mass flow by keeping burner power constant. It is observed that the effect of the secondary air increase with decreases in equivalence ratio. It is found that the flame takes different shapes; for example, it takes a conical shape for ϕ = 0.3–0.5. For a lower equivalence ratio of 0.2, the flame diameter reduces and shape changes from conical to a "V" shaped flame. This is due to a change in flame stabilization location on the central chamber combustion to the outer burner lips, well documented by the previous study of S. Candel [57].

Fig. 7 shows the effect of increasing the swirl number (for different equivalence ratios (ϕ)) on the velocity for the biogas doped with 40% H_2.

The data shows that the recirculation zones are formed closer to the inlet section and in the middle of the combustion chamber. These zones enhance the stability of flames by recycling and remixing the hot gases with cold reactants, which produce a durable flame. The swirl number (SN) increases the vortex in the middle of the combustion chamber and decreases the vortex in the chamber's corners, especially for SN = 1.19. Further, an increase in the central recirculation zone indicates proper mixing of fuel and air, that increase may be because of two reasons, first because of the enhance and the increase in swirl velocity, especially the tangential flow velocity component (1.88 to 4.90), for (ϕ = 0.5 to 0.2), respectively. Secondly, the deflection of the flow from the central axis of the chamber creates a low pressure in this zone, which increases the size of the vortex in the center of the combustor.

Effects of H_2 enrichment and equivalence ratio on temperature

The average static temperature profiles along the central axis of the combustion chamber for the biogas and biogas doped with H_2 is shown in Fig. 8(a,b,c,d).

Biogas (CH_4 = 60%, CO_2 = 40%) is utilized as the fuel reference. For Fig. 8 (a,b), when the hydrogen is added, the temperature reaches the maximum temperature (1557 K-1164 K) height of 0.1 m-0.75 m for 50% H_2 at (ϕ = 0.5,0.2), respectively. Additionally, the temperature in the absence of hydrogen reaches the maximum (1517 K-1143 K) at 0.1 m-0.75 m for the (ϕ = 0.5,0.2), respectively. Here the peak temperatures increased by (40–21 K) from the biogas reference to biogas with 40% H_2 additions at (ϕ = 0.5, 0.2), respectively. As well, there is a significant impact after Z = 0.10 m in the secondary zone of dilution air. Therefore, the temperature of the unburnt fuel decreases due to the secondary airflow, and this influence gets more significant when the ϕ reduces. The result reveals that the temperature increases with hydrogen increase, which means the hydrogen accelerates combustion reaction.

Fig. 8 (c) shows an increase in the temperature of the biogas reference, and the biogas blended with 40% H_2 when the (ϕ) increases. It is observed that almost the flame temperature at ϕ equal 0.2 with a high rate of hydrogen (40% H_2) close to the results of the pure biogas (0 % H_2), whereas for an ϕ superior of 0.2, the temperature of hydrogen added to the biogas increases, that due to the secondary air a significant impact at an ϕ = 0.2, with low flame temperature. It is observed that a decrease in the temperature with increases in the swirl number (0.74–1.19) and decreases in the equivalence ratio (0.5–0.2); because of the improvements in Swirl Number (SN) leads the fuel–air mixture streams increases and that makes the fuel consumed as it presents in Fig. 8(d).

Fig. 8(d) shows the axial mixture fraction for the biogas doped with 40% H_2. It is observed that the mixture fraction decreases when the Swirl Number (SN) increases, and the (ϕ) decreases, which indicates mixing development; fuel consumption due to combustion. From equation (16), it is shown that when the air mass flow increases while keeping the mass flow of fuel constant, the mixture fraction will decrease, and vice versa, which is in agreement with Fig. 8 (d).

Fig. 9 (a-b) studied the maximum temperature for different values of H_2 added to the biogas and different equivalence ratios.

The maximum temperatures increase with an increase in the H_2 addition and with an increase in the ϕ. It is observed that the difference in the temperature when H_2 is added decreases as the equivalence ratio decreases. The highest gradient of the maximum static temperature

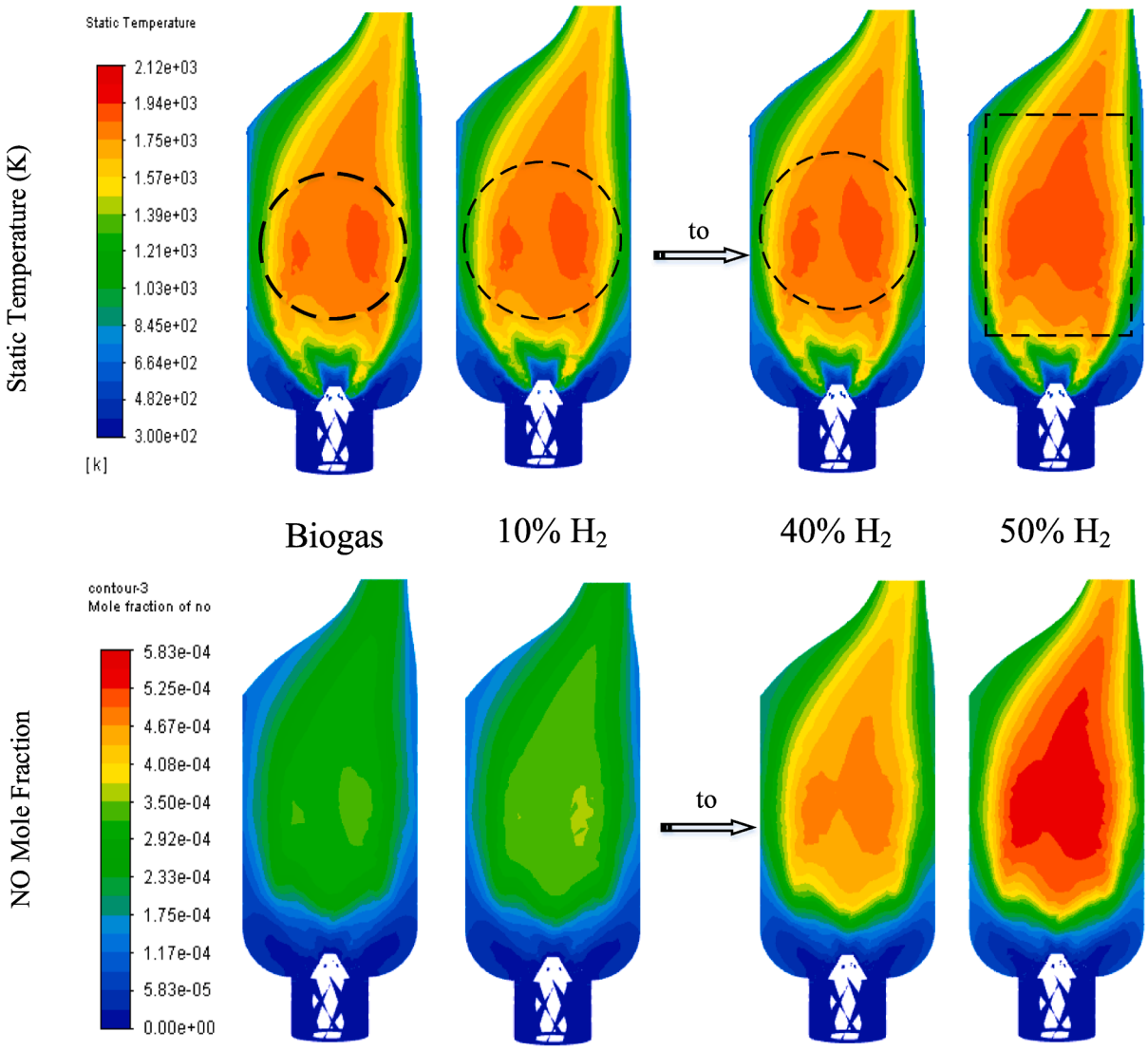

Fig. 4. A sequence of images describing the biogas flame temperature distributions [K] (above) and NO emissions (below), with different rates of hydrogen concentration by Vol%.

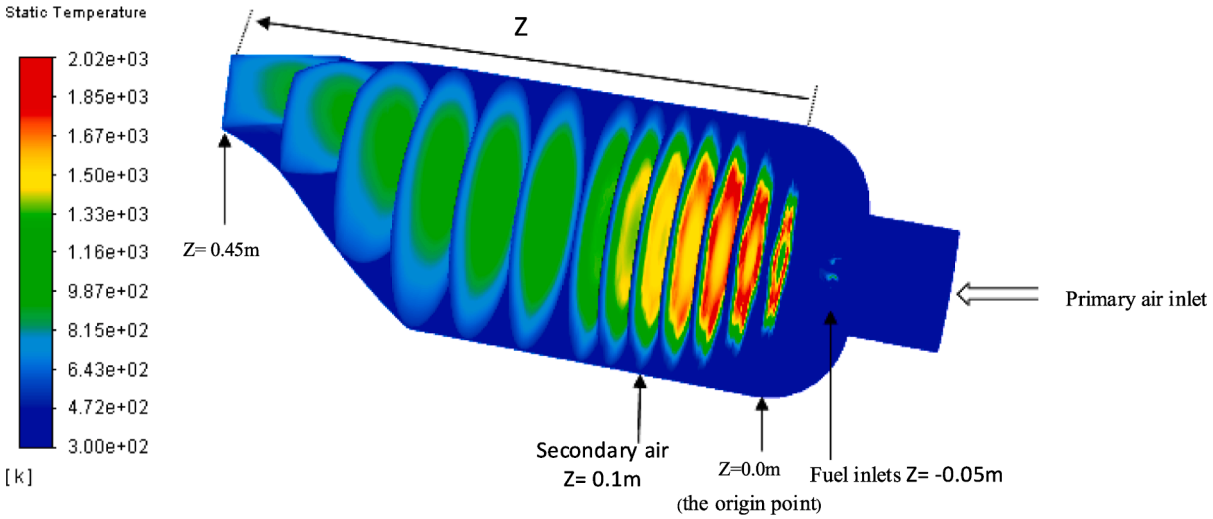

Fig. 5. Flame temperature distributions cross-sections for 50% H_2 hydrogen rate.

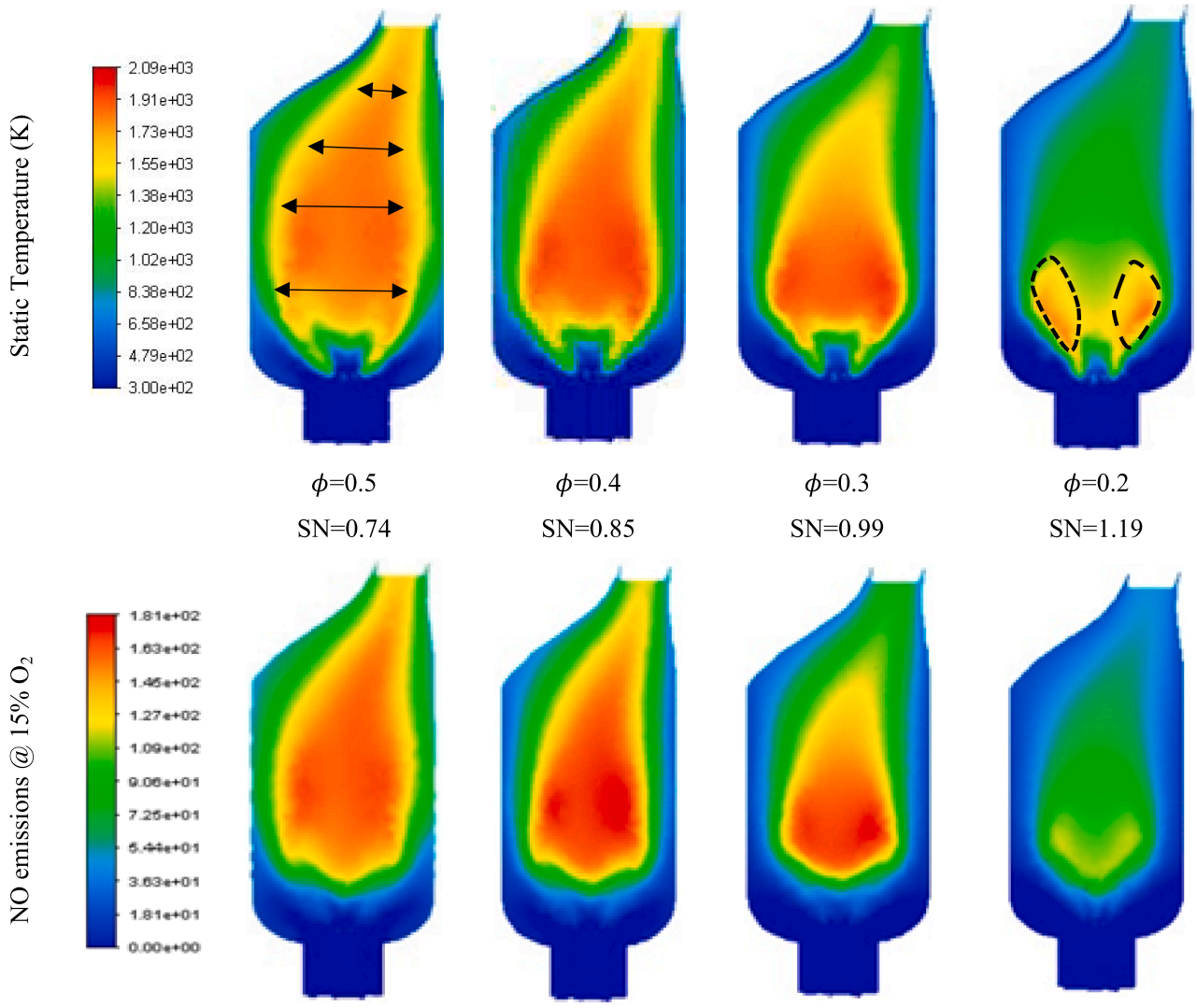

Fig. 6. Comparison of flames temperature distributions and NO emissions, with different values of equivalence ratio: ϕ = 0.3–0.5 (CF: conical flame shape), ϕ = 0.2 (VF: "V" shaped flame).

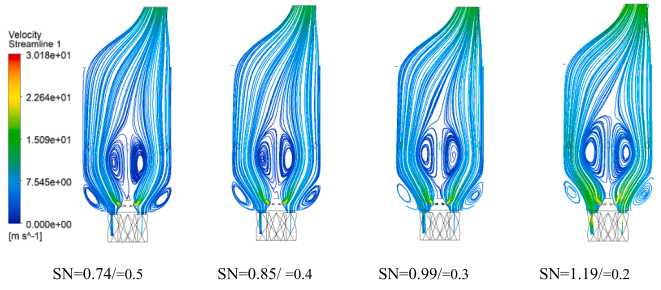

Fig. 7. Velocity streamlines for 40% H_2 hydrogen rate, with different values of equivalence ratio: ϕ = 0.5–0.2 and different values of swirl number: 0.74–1.19.

between ϕ = 0.3 and ϕ = 0.2. This is due to the increased reaction rate due to the increase in the radical pool, such as OH radicals (refer to Fig. 14 (c) for more details).

Effects of H_2 addition and equivalence ratio on NO emissions

The thermal and prompt NO emissions profiles are displayed in Fig. 10. The NO thermal used the reaction no. (28), and it is given below. Furthermore, the NOx formation is determined by how N_2 is broken down, and the hard part of NO formation is not the intermediate species forming NO or NO_2. The hardest part of NOx formation is to break the triple bond of the N_2 molecule.

In this case, to estimate the different NO mechanisms, each mechanism was isolated by disabling only those breaking down N_2 in each route. For example, for NO, there are three reactions as follows:

$$O + N_2 = N + NO \quad (29)$$

$$N + O_2 = O + NO \quad (30)$$

$$N + OH = H + NO \quad (31)$$

In order to determine the thermal NO, the reaction (28) should be disabled because the intermediate species through other NO routes will still be generated and follow these reactions [58–60]. Furthermore, it has been confirmed in Fig. 10 (c), where it can observe that match the result of three reactions and when using a single reaction (28). NO thermal increases as hydrogen in the biogas mixture increases from 0% to 50% by volume at ϕ = 0.5, due to the higher flame temperature shown in Fig. 8 (a), whereas the NO prompt decreases after injection zone, and this because of the reduction in the CH concentration, as discussed in the context of Fig. 11.

The impact of the biogas-H_2 blend on the distribution of NO

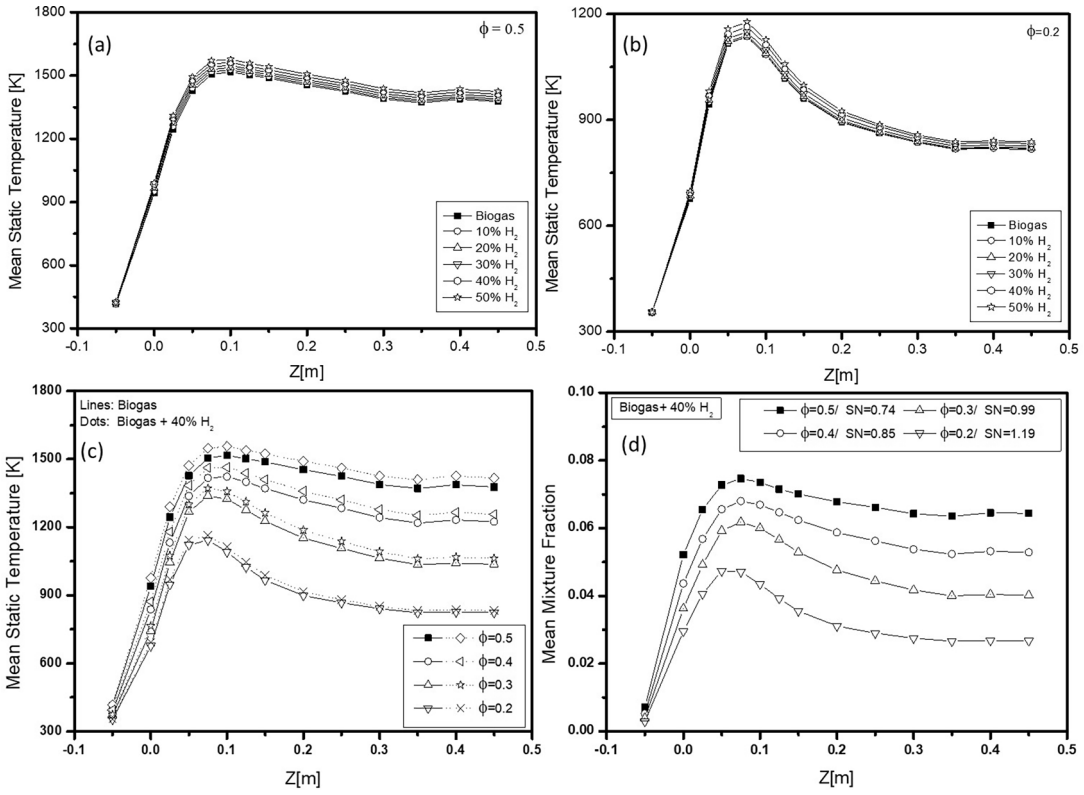

Fig. 8. Axial stemperature profiles at different hydrogen concentrations (a) ϕ = 0.5, (b) ϕ = 0.2, and (c) at different ϕs for biogas and 40% H_2-Biogas (d) mixture fraction for 40% H_2 at different ϕs/ SN.

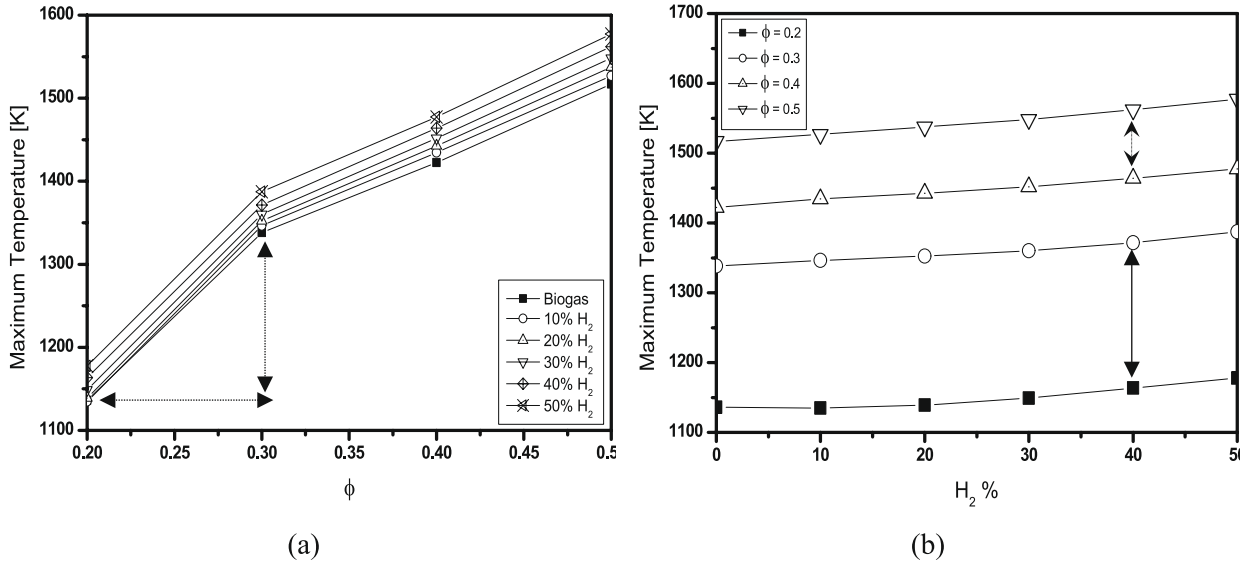

Fig. 9. Maximum static temperature profiles (a) at different ϕs (b) at different hydrogen concentrations (H_2%).

emissions is shown in Fig. 11. The addition of hydrogen leads to an increase in the flame temperature and will promote the NO formation substantially in the injection zone.

Thus, it is shown that at ϕ = 0.2, the NO peak is formed, and this peak slightly reduced along the axis, while at ϕ = 0.5, it maintained constant. It may be due to the increase in the equivalence ratio and the weak effect of the secondary air extended into the flame inside the chamber. It is an essential factor in forming NO-thermal and NO-prompt, or the formation of HCN, C_2H_2. It is also observed that the formation of the relative peak for NO is higher for ϕ equal to 0.2 with hydrogen addition compared to ϕ = 0.5. Peak NO varies as the amount of H_2 in biogas increases from 10 to 50% by volume. This could explain that the addition of H_2 decreases the NO-prompt because the CH concentration is reduced and the effect of the triple-bond contained in the formation of the NO-prompt mechanism. The different routes for NOx formation are determined by breaking down the triple-bond of N_2 molecule, whereas the NO-thermal increases due to the higher temperature in these flames, as shown in Fig. 10(a).

Fig. 12 (a, b) display the maximum NO emissions distribution for different values of H_2 added to the biogas and different equivalence

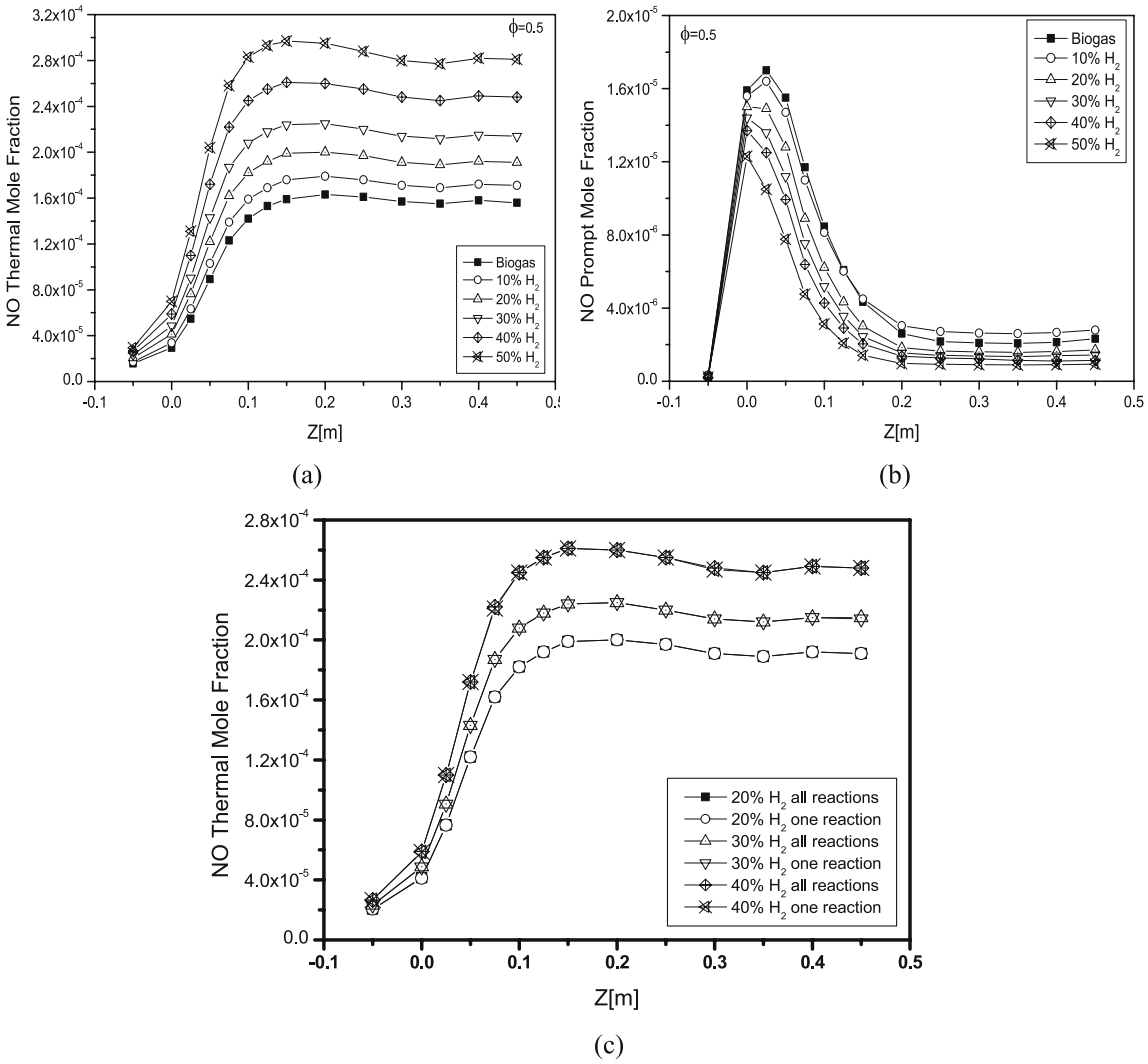

Fig. 10. Axial NO mole fraction profiles (a) NO thermal and (b) NO prompt (c) comparison the reaction of NO thermal.

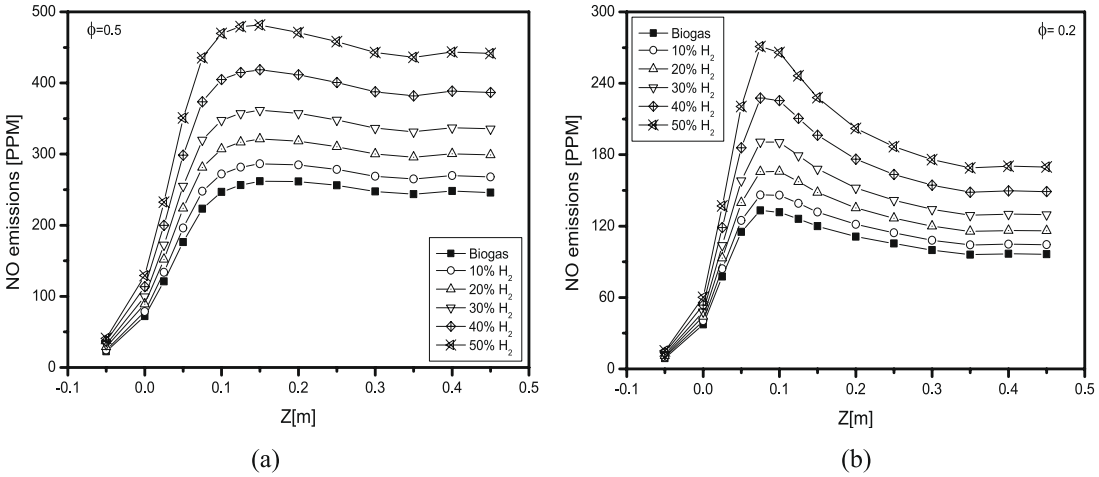

Fig. 11. Axial NO emissions profiles at different hydrogen concentrations (a) $\phi = 0.5$, (b) $\phi = 0.2$.

ratios. It is shown that the maximum magnitude of NO (ppm @ 15 vol% O_2) increases with the increase in the hydrogen addition in the biogas and with the increase in the equivalence ratio of 0.2 to 0.5. A critical observation is that NO emissions are smaller at a low H_2 enrichment % and low ϕ. According to the literature, NO decreases by increasing the swirl number [61–63]. These observations from the past are in line with current NOx emission results shown in Fig. 12 (b,c).

Fig. 12 (c) shows the maximum NO emissions in the outlet chamber

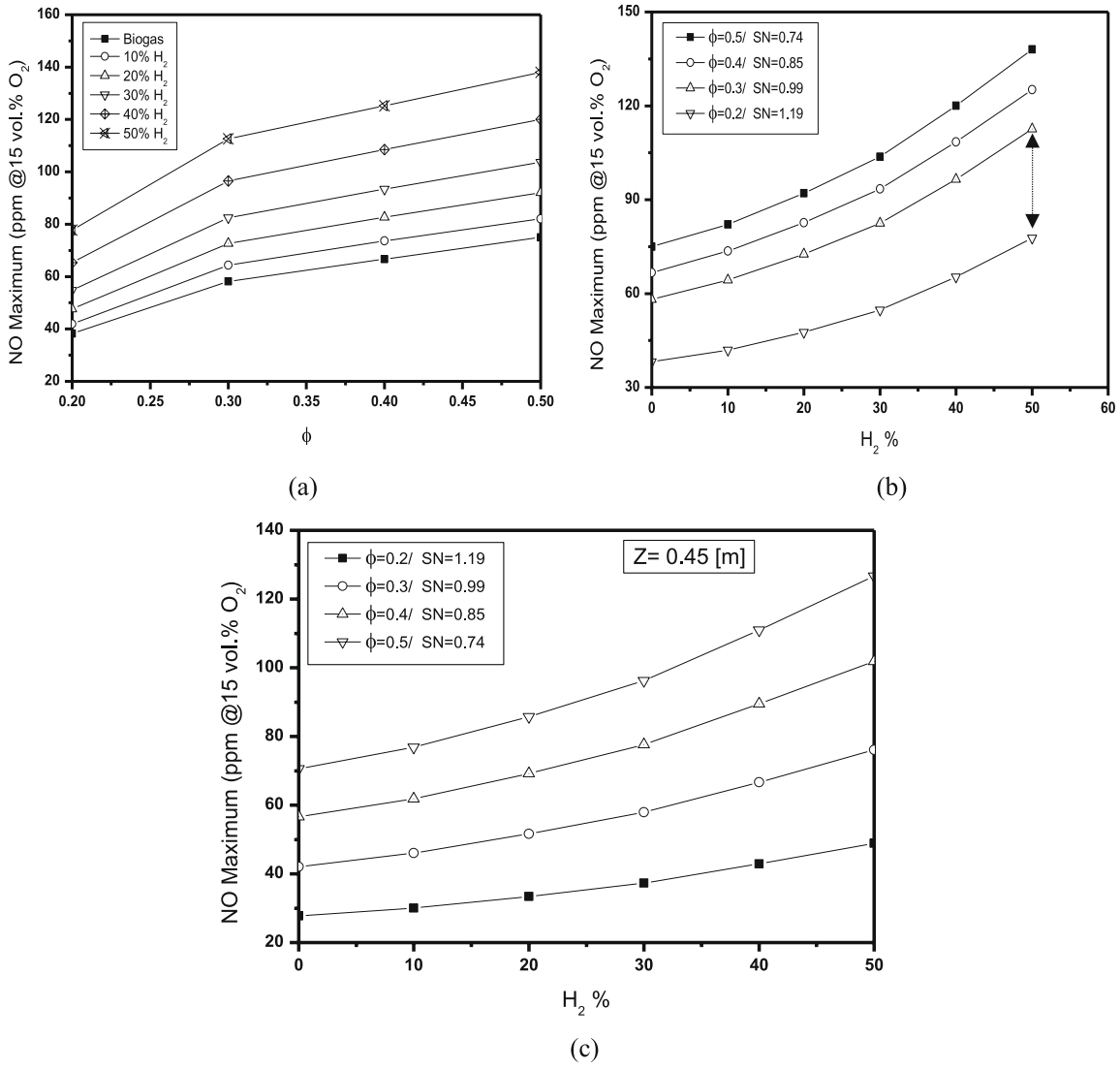

Fig. 12. Maximum NO emissions profiles at different hydrogen concentrations (a) at different ϕs (b) at different hydrogen concentrations (H_2 %) and (c) different (H_2 %) at Z = 0.45 m.

Table 5
NO maximum emissions in the outlet chamber (ppm @15 vol% O2).

	Biogas	10%H_2	20% H_2	30% H_2	40%H_2	50%H_2
ϕ = 0.2	28.0829	30.5699	33.9896	38.0311	43.3161	**49.2228**
ϕ = 0.3	42.3834	46.4249	52.0207	58.2383	66.943	76.5803
ϕ = 0.4	56.6839	61.9689	69.7409	**77.8238**	89.9482	102.383
ϕ = 0.5	**70.3627**	76.8912	85.9067	96.4767	110.777	126.943
Average	**49.378225**	53.963725	60.414475	67.642475	77.746075	88.782275

(ppm @15 vol% O_2), and their values are summarized in Table 5.

At the same time, when enhancing the combustion characteristics by using hydrogen/biogas mixture, the NO emissions increase. In order to compensate for this deficiency, the optimum condition on the equivalence ratio and the hydrogen enrichment % are identified from these Fig. 12(a,b,c). It is observed that the lower NO emissions values are recorded for the pure biogas combustion (0.0%H_2). In comparison, it increases from (28 to 70 ppm) at (ϕ = 0.2 to 0.5), with an average value of 49.38 ppm @15 vol% O_2. The NOx emission value for the case of 50% H_2/biogas at ϕ = 0.2 with its temperature equal 1175 K is close to pure biogas at ϕ = 0.3. Therefore, this mixture can be considered the optimal fuel for the can-type combustor. At ϕ ≤ 0.4 and below 30% H_2 (less than 77.8238 ppm @15 vol% O_2) also acceptable with temperature less than 1450 K, that because the NOx level ≤ 75 ppm at @15 vol% O_2 is the New Source Performance Standards (NSPS) of the united states required for any utility gas turbine engine [64]. Therefore, the optimal mixtures will help flame stabilization, consistent power output, and low NO emissions, similar to what is usually achieved by the gas turbine engine fuels. Also, these temperatures can produce a satisfactory output power and reduce the turbine blade cooling power required.

Effects of H_2 addition on CO and CO_2 emission

Fig. 13(a,b,c,d) demonstrates the CO and CO_2 concentrations along the central axis of the combustor. It is shown that the CO formation increases in the primary zone. This is due to incomplete fuel combustion

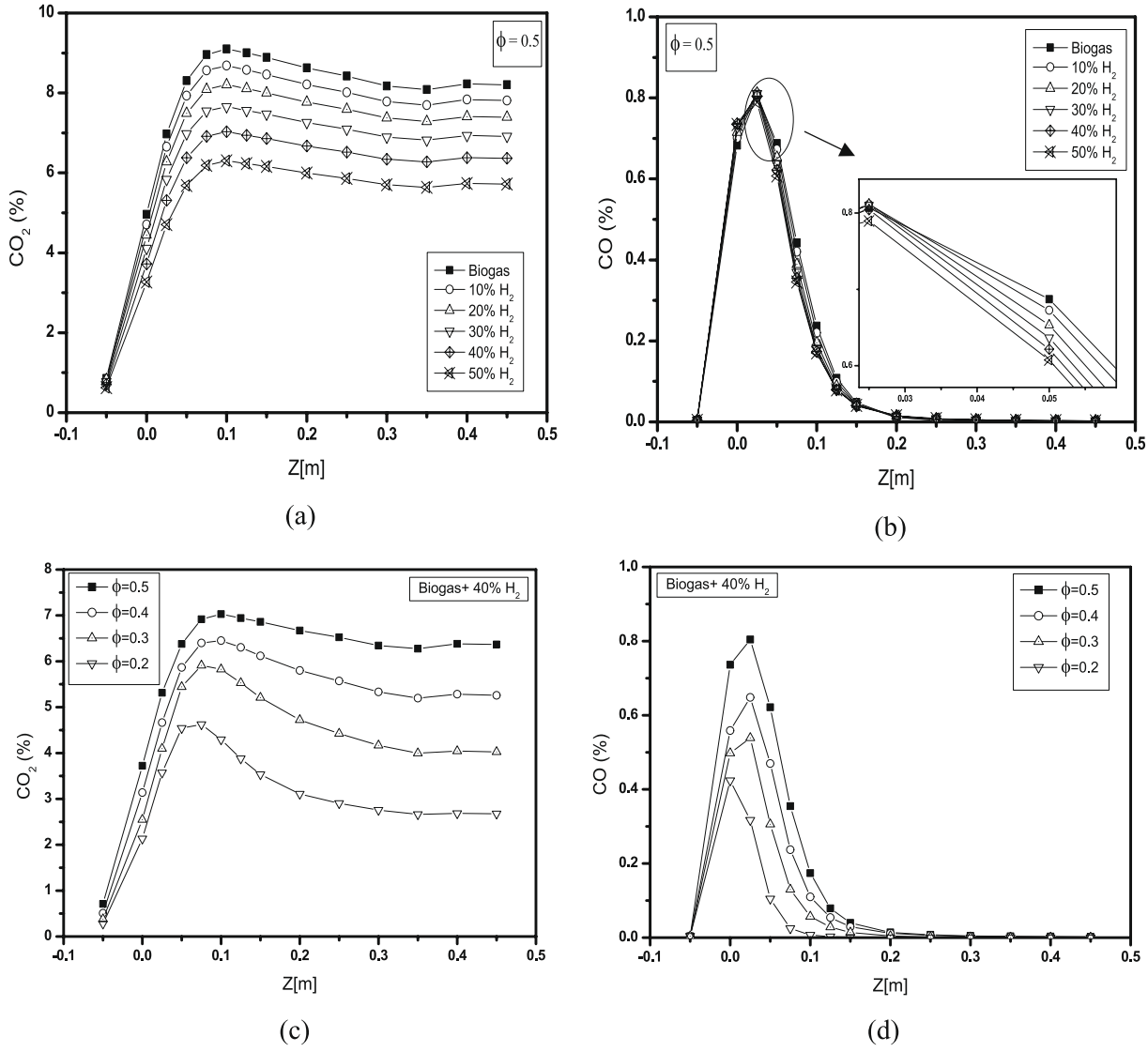

Fig. 13. Axial concentration of CO_2 and CO profiles (a,b) at different H_2%, and $\phi = 0.5$ (c,b) at 40 H_2 % and different ϕs.

in the primary zone.

Then the CO emissions decrease until the chamber outlet. The considerable reduction of CO emissions in the second reaction zone may be attributed to the increase in the OH radical, favouring CO oxidation to CO_2. It is also shown in this Fig. 13 (a,b,c,d), CO_2 emission decreases with the hydrogen rate increases in the fuel mixture. The percentage of CO reduces dramatically with the addition of hydrogen. This can mainly be due to two reasons; firstly, the quantity of carbon in the fuel mixture decreases with increasing hydrogen rate because of the hydrogen addition. Secondly, hydrogen addition increases the OH radical concentration in the flame, which is the dominant radical for CO mole oxidation, and these results agree with Fig. 14 (c) (refer to Ali and Varunkumar[19] on the details related to CO oxidation pathways).

Effects of the equivalence ratio on CH_4, H_2, OH, and O_2

The profiles of CH_4, H_2, OH and O_2 mole fractions of hydrogen-biogas mixture combustion are presented in Fig. 14(a,b,c,d).

In biogas + 40% H_2, the mole fraction of CH_4 and H_2 peaks near the injector zone for ϕ equal to 0.5 and then decreases with the axial distance. Furthermore, the hydrogen enrichment leads to an essential increase in the radicals H and OH in the mixture. Moreover, the effect of hydrogen addition on the O_2 mole fraction is studied. In the zone near the secondary air, it is noted that the mole fraction of O_2 started to increase, and there was a reduction in CH_4. It is concluded that hydrogen has an essential effect on the reaction zone and, therefore, significantly impacts the flame thickness. A comparison is made between the pure biogas and biogas + 40% H_2 mixture and results presented in Fig. 14 (a, b,c,d). Fig. 14 (a) shows that the CH_4 mole fraction for pure biogas is more than the case of 40 %H2, which makes sense because pure biogas contains 60% CH_4 and only 36% CH_4 for the biogas doped by 40 %H_2. The OH mole fraction represents the flame macrostructure, which peaks close to the inlet section at which the flame is stabilized, as in Fig. 14 (c). It can be observed from Fig. 14 (d) that the H_2 mole fraction for pure biogas is less than 40% H_2 addition. This is because the pure biogas does not contain hydrogen in its compositions. As for the ratio of hydrogen are caused by interactions between the compositions.

Conclusion and future work

This paper has presented an investigation on the effects of hydrogen blending to biogas mixture, and equivalence ratio/swirl number on the stable flame operation, the temperature distribution, temperature contours, and velocity streamlines contours, emissions of NO, and species concentrations. The burner power is kept constant at 60 kW, the equivalence ratio is varied from 0.2 to 0.5, and biogas blended with

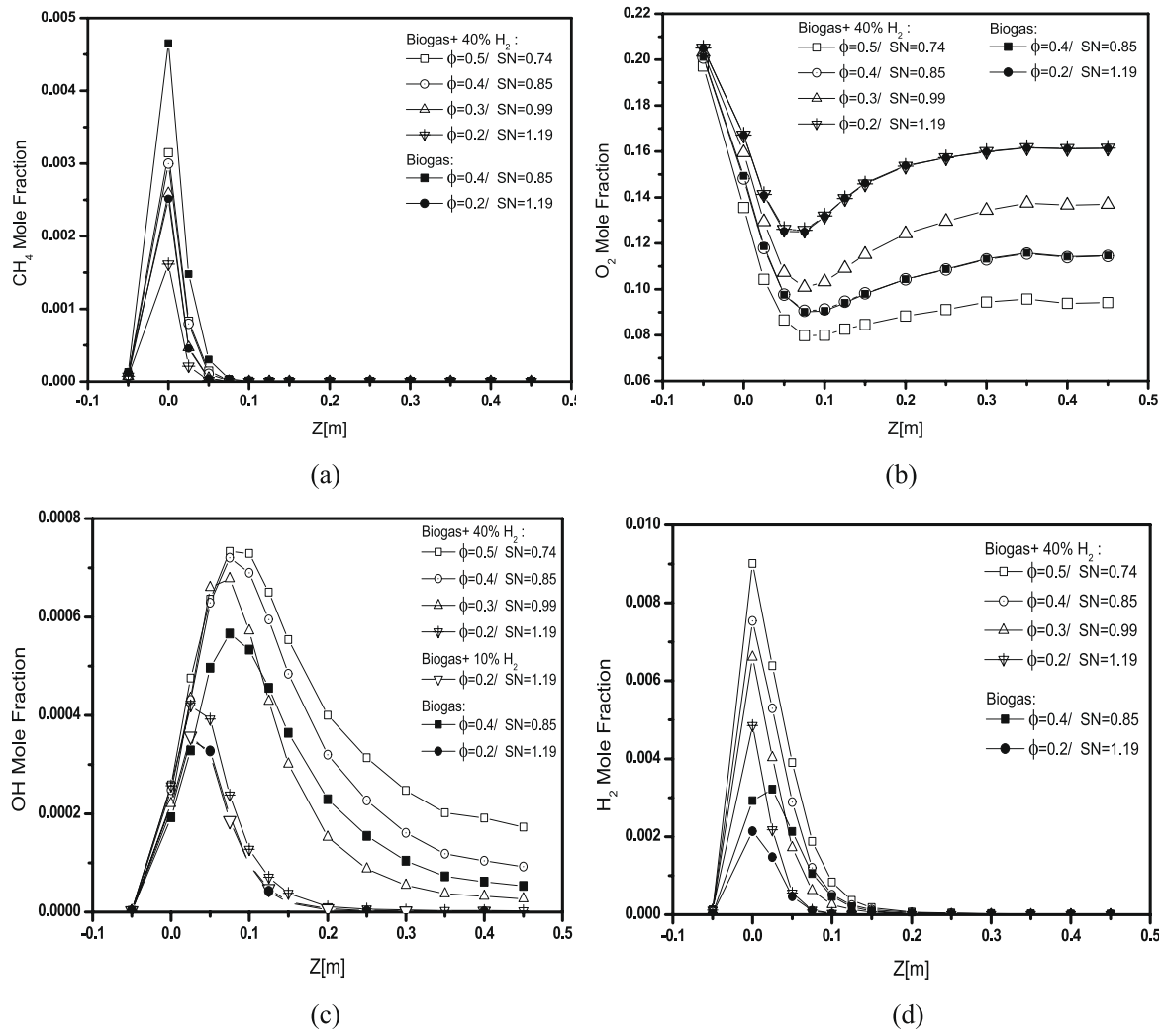

Fig. 14. Axial mole fractions profiles at different ϕs, and 40 H_2 % of (a) CH_4 mole fraction (b) O_2 mole fraction (c) OH mole fraction, and (d) H_2 mole fraction.

hydrogen at different compositions (0% to 50%). The k-ε standard and steady laminar flamelet (SLF) models are used to study the non-premixed flame generated by the combustion of the biogas-hydrogen on the can-type combustor. The numerical model displays that the results are in good accord with available data in the literature. The most important conclusions of this study can be summarized as follows:

- The addition of H_2 in biogas improves the flame stabilization and the emissions (which reinforces the reaction zone). The length and the thickness of the biogas flame are expanded when hydrogen is introduced to the fuel mixture. Similar effects were observed with increasing ϕ.
- The optimum proportion of hydrogen and equivalence ratio for the combustor chamber is 50% H_2 for $\phi = 0.2$, with its temperature equal to 1175 K. At these conditions, the flame temperature and the NO emissions are close to the results of pure biogas at the same equivalence ratio and much less for the equivalence ratio in the range of 0.3–0.5.
- At $\phi \leq 0.4$ and below 30% H_2, the biogas/hydrogen mixture is acceptable and will help flame stabilization, reasonable power output, and low NOx emissions, similar to what is usually achieved by the gas turbine engine fuels.
- The decrease in the equivalence ratio leads to increases in the swirl number; this allows for creating the recirculation zone established, enhancing the flame stabilization.
- Reduces the maximum flame temperature when operating at extra-lean conditions ($\phi = 0.5$ to 0.2) with the presence of hydrogen will decrease the hot zone temperature, reducing the thermal NOx.
- The increase in the swirl number and decrease of equivalence ratio causes a reduction in the flame macrostructure in length and flame thickness. This allows the expansion of a surface area for the flame's heat exchange with the chamber wall, especially with the secondary air.
- Higher swirl numbers lead to improved premixing between air and fuel streams due to increasing the tangential flow velocity and the deflection of the flow from the chamber's central axis, increasing the size of the vortex in the center of the combustor.
- Zones of air dilution play an essential role in flame stabilization, which reduces NOx and CO formation.

Upgrading syngas to have hydrogen and mixing it with biogas gives a good alternative for fossil fuels. This mixture can be investigated in the future, along with the thermoacoustic instabilities of gas turbine combustors.

CRediT authorship contribution statement

Sabrina Benaissa: Methodology, Software, Validation, Writing – original draft. **Belkacem Adouane:** Supervision, Conceptualization. **S. M. Ali:** Supervision, Formal analysis, Investigation, Writing- review &

editing. **Sherid S. Rashwan:** Software, Writing- review & editing. **Z. Aouachria:** Supervision

Declaration of Competing Interest

The authors declare that they have no known competing financial interests or personal relationships that could have appeared to influence the work reported in this paper.

References

[1] D.W. Keith, G. Holmes, D. St. Angelo, K. Heidel, A Process for Capturing CO2 from the Atmosphere, Joule. 2 (2018) 1573–1594. https://doi.org/https://doi.org/10.1016/j.joule.2018.05.006.

[2] M.A. Nemitallah, S.S. Rashwan, I.B. Mansir, A.A. Abdelhafez, M.A. Habib, Review of novel combustion techniques for clean power production in gas turbines, Energy & Fuels. 32 (2) (2018) 979–1004, https://doi.org/10.1021/acs.energyfuels.7b03607.

[3] G. Lazaroiu, E. Pop, G. Negreanu, I. Pisa, L. Mihaescu, A. Bondrea, V. Berbece, Biomass combustion with hydrogen injection for energy applications, Energy 127 (2017) 351–357, https://doi.org/10.1016/j.energy.2017.03.133.

[4] C. Diaz-Gonzalez, A.-A. Arrieta, J.-L. Suarez, Comparison of combustion properties of simulated biogas and methane, Ciencia, Tecnologia y Futuro 3 (2009).

[5] E. Porpatham, A. Ramesh, B. Nagalingam, Effect of hydrogen addition on the performance of a biogas fuelled spark ignition engine, International Journal of Hydrogen Energy. 32 (2007) 2057–2065. doi: 10.1016/j.ijhydene.2006.09.001.

[6] E. Porpatham, A. Ramesh, B. Nagalingam, Effect of compression ratio on the performance and combustion of a biogas fuelled spark ignition engine, Fuel. 95 (2012) 247–256. doi: 10.1016/j.fuel.2011.10.059.

[7] S.S. Rashwan, M.A. Nemitallah, M.A. Habib, Review on premixed combustion technology: stability, emission control, applications, and numerical case study, Energy Fuels 30 (12) (2016) 9981–10014, https://doi.org/10.1021/acs.energyfuels.6b02386.

[8] F. Teng, The Effect of Hydrogen Concentration on the Flame Stability and Laminar Burning Velocity of Hydrogen-Hydrocarbon-Carbon Dioxide Mixtures, University of Sheffield, 2014.

[9] J.W. Sheffield, An outlook of hydrogen as an automotive fuel, Int. J. Hydrogen Energy. 14 (7) (1989) 449–474.

[10] S. Benaissa, B. Adouane, S.M. Ali, A. Mohammad, Effect of hydrogen addition on the combustion characteristics of premixed biogas/hydrogen-air mixtures, International Journal of Hydrogen Energy. 46 (2021) 18661–18677. doi: 10.1016/j.ijhydene.2021.02.225.

[11] C.D. Rakopoulos, C.N. Michos, E.G. Giakoumis, Studying the effects of hydrogen addition on the second-law balance of a biogas-fuelled spark ignition engine by use of a quasi-dimensional multi-zone combustion model, Proc. Inst. Mech. Eng., Part D: J. Automobile Eng. 222 (11) (2008) 2249–2268.

[12] G. JUSTE, Hydrogen injection as additional fuel in gas turbine combustor. Evaluation of effects, Int. J. Hydrogen Energy. 31 (14) (2006) 2112–2121.

[13] K.K. Gupta, A. Rehman, R.M. Sarviya, Bio-fuels for the gas turbine: a review, Renewable and Sustainable Energy Reviews. 14 (9) (2010) 2946–2955.

[14] N. Kobayashi, T. Mano, N. Arai, Fuel-rich hydrogen-air combustion for a gas-turbine system without CO2 emission, Energy 22 (2-3) (1997) 189–197.

[15] A.A. Hairuddin, T. Yusaf, A.P. Wandel, A review of hydrogen and natural gas addition in diesel HCCI engines, Renewable and Sustainable Energy Reviews. 32 (2014) 739–761.

[16] H.A. Alrazen, A.R. Abu Talib, R. Adnan, K.A. Ahmad, A review of the effect of hydrogen addition on the performance and emissions of the compression–Ignition engine, Renewable and Sustainable Energy Reviews. 54 (2016) 785–796.

[17] Z. Wei, H. Zhen, C. Leung, C. Cheung, Z. Huang, Effects of unburned gases velocity on the CO/NO2/NOx formations and overall emissions of laminar premixed biogas-hydrogen impinging flame, Energy 196 (2020), 117146.

[18] H.S. Zhen, C.W. Leung, C.S. Cheung, Z.H. Huang, Characterization of biogas-hydrogen premixed flames using Bunsen burner, International Journal of Hydrogen Energy. 39 (2014) 13292–13299. doi: 10.1016/j.ijhydene.2014.06.126.

[19] S.M. Ali, S. Varunkumar, Effect of burner diameter and diluents on the extinction strain rate of syngas-air non-premixed Tsuji-type flames, International Journal of Hydrogen Energy. 45 (15) (2020) 9113–9127.

[20] S.M. Ali, A Three-step Global Kinetic Mechanism for Predicting Extinction Strain Rate of Syngas-air Nonpremixed Flames, Combustion Science and Technology. (2020) 1–24.

[21] Z.L. Wei, C.W. Leung, C.S. Cheung, Z.H. Huang, Effects of equivalence ratio, H2 and CO2 addition on the heat release characteristics of premixed laminar biogas-hydrogen flame, Int. J. Hydrogen Energy. 41 (2016) 6567–6580. doi: 10.1016/j.ijhydene.2016.01.170.

[22] A. Mameri, F. Tabet, Numerical investigation of counter-flow diffusion flame of biogas–hydrogen blends: effects of biogas composition, hydrogen enrichment and scalar dissipation rate on flame structure and emissions, Int. J. Hydrogen Energy 41 (2016) 2011–2022.

[23] N. Jalalatian, S. Tabejamaat, B. Kashir, M. EidiAttarZadeh, An experimental study on the effect of swirl number on pollutant formation in propane bluff-body stabilized swirl diffusion flames, Phys Fluids 31 (2019) 55105.

[24] A. Kotb, H. Saad, Case study for co and counter swirling domestic burners, Case Stud. Thermal Eng. 11 (2018) 98–104.

[25] I. Yılmaz, Effect of swirl number on combustion characteristics in a natural gas diffusion flame, J. Energy Resour. Technol. 135 (2013).

[26] N. Peters, Laminar diffusion flamelet models in non-premixed turbulent combustion, Prog. Energy Combustion Sci. 10 (3) (1984) 319–339.

[27] H.S. Zhen, Z.L. Wei, Z.B. Chen, M.W. Xiao, L.R. Fu, Z.H. Huang, An experimental comparative study of the stabilization mechanism of biogas-hydrogen diffusion flame, Int. J. Hydrogen Energy 44 (3) (2019) 1988–1997.

[28] V. Kumar Yadav, A. Ray, M.R. Ravi, Experimental and computational investigation of the laminar burning velocity of hydrogen-enriched biogas, Fuel. 235 (2019) 810–821. doi: 10.1016/j.fuel.2018.08.068.

[29] Z. Wei, H. Zhen, J. Fu, C. Leung, C. Cheung, Z. Huang, Experimental and numerical study on the laminar burning velocity of hydrogen enriched biogas mixture, Int. J. Hydrogen Energy 44 (39) (2019) 22240–22249.

[30] W.C. Nadaleti, G. Przybyla, Emissions and performance of a spark-ignition gas engine generator operating with hydrogen-rich syngas, methane and biogas blends for application in southern Brazilian rice industries, Energy 154 (2018) 38–51, https://doi.org/10.1016/j.energy.2018.04.046.

[31] A. Fluent, 12.0 Theory Guide, Ansys Inc. 5 (2009) 15.

[32] T. Poinsot, D. Veynante, Theoretical and numerical combustion, RT Edwards, Inc., 2005.

[33] H.K. Versteeg, W. Malalasekera, An introduction to computational fluid dynamics: the finite volume method, Pearson education, 2007.

[34] N. Peters, Turbulent combustion, (2001).

[35] N. Oumrani, M. Aouissi, A. Bounif, B. Yssaad, F. Tabet, I. Gokalp, A first-and second-order turbulence models in hydrogen non-premixed flame, Int. J. Heat Technol. 33 (3) (2015) 27–34.

[36] A. Obieglo, PDF modeling of H2 and CH4 chemistry in turbulent nonpremixed combustion, Eidgenössische Technische Hochschule Zürich (2000).

[37] B.E. Launder, N.D. Sandham, Closure strategies for turbulent and transitional flows, Cambridge University Press, 2002.

[38] L. Wang, D.C. Haworth, S.R. Turns, M.F. Modest, Interactions among soot, thermal radiation, and NOx emissions in oxygen-enriched turbulent nonpremixed flames: a computational fluid dynamics modeling study, Combustion and Flame 141 (2005) 170–179.

[39] M.F. Modest, Radiative Heat Transfer, Academic press, 2013.

[40] J.G. Speight, Chapter 10 - Combustion of Hydrocarbons, in: J.G. Speight (Ed.), Handbook of Industrial Hydrocarbon Processes, Gulf Professional Publishing, Boston, 2011: pp. 355–393. https://doi.org/https://doi.org/10.1016/B978-0-7506-8632-7.10010-6.

[41] M.A. Abdel-Hadi, A simple apparatus for biogas quality determination, Misr. J. Ag. Eng. 25 (2008) 1055–1066.

[42] N. Grech, C. Koupper, P.K. Zachos, V. Pachidis, R. Singh, Considerations on the numerical modeling and performance of axial swirlers under relight conditions, J. Eng. Gas Turbines Power 134 (2012).

[43] S. Taamallah, K. Vogiatzaki, F.M. Alzahrani, E.M.A. Mokheimer, M.A. Habib, A. F. Ghoniem, Fuel flexibility, stability and emissions in premixed hydrogen-rich gas turbine combustion: technology, fundamentals, and numerical simulations, Appl. Energy 154 (2015) 1020–1047.

[44] O.A. Marzouk, E.D. Huckaby, Simulation of a swirling gas-particle flow using different k-epsilon models and particle-parcel relationships, Eng. Lett. 18 (2010).

[45] A.R. Norwazan, M.N.M. Jaafar, Studies of isothermal swirling flows with different RANS models in unconfined burner, in: World Congress on Sustainable Technologies (WCST-2014), IEEE, 2014: pp. 48–53.

[46] G.P. Smith, D.M. Golden, M. Frenklach, B.E. N. W. Moriarty, M. Goldenberg, C.T. Bowman, R.K. Hanson, S. Song, W.C.G. Jr., V. V Lissianski, Z. Qin, GRI mech 3.0, (2000). http://www.me.berkeley.edu/gri_mech/.

[47] C. Ghenai, Combustion of syngas fuel in gas turbine can combustor, Mech. Eng. 2010 (2010) 13.

[48] H. Pathan, K. Partel, V. Tadvi, Numerical investigation of the combustion of methane air mixture in gas turbine can-type combustion chamber, Int. J. Scientific Eng. Res. 3 (2012) 1–7.

[49] P. Koutmos, J.J. McGuirk, Isothermal flow in a gas turbine combustor—a benchmark experimental study, Experiments in Fluids. 7 (5) (1989) 344–354.

[50] C.H.U. Praveen, A.H.K. Yadav, Numerical simulation of gas turbine can combustor engine, Int. J. Eng. Res. General Sci. 3 (2015) 192–201.

[51] H.-Y. Shih, C.-R. Liu, Combustion characteristics of a can combustor with a rotating casing for an innovative micro gas turbine, J. Eng. Gas Turbines and Power. 131 (2009) 41501.

[52] G.C. Krieger, A.P.V. Campos, M.D.B. Takehara, F. Alfaia da Cunha, C.A. Gurgel Veras, Numerical simulation of oxy-fuel combustion for gas turbine applications, Appl. Thermal Eng. 78 (2015) 471–481.

[53] N.H. Gor, M.J. Pandya, Analysis of Can Type Combustion Chamber–A Review, (n. d.).

[54] M. Andersson, A. Larsson, A.M. Carrera, Pentane rich fuels for standard Siemens DLE gas turbines, in: Turbo Expo: Power for Land, Sea, and Air, 2011: pp. 905–916.

[55] C. Ghenai, I. Janajreh, Combustion of Renewable Biogas Fuels, Combustion of Renewable Biogas Fuels. (2015) 831.

[56] C. Ghenai, Combustion and Emissions Performance of Syngas Fuels Derived from Palm Kernel Shell and Polyethylene (PE) Waste via Catalytic Steam Gasification, World Academy of Science, Engineering and Technology, International Journal of Mechanical, Aerospace, Industrial, Mechatronic and Manufacturing Engineering. 9 (2015) 1024–1030.

[57] S. Candel, D. Durox, S. Ducruix, A.-L. Birbaud, N. Noiray, T. Schuller, Flame dynamics and combustion noise: progress and challenges, Int. J. Aeroacoustics. 8 (1) (2009) 1–56.

[58] G. Irvin, Y. Richard, Combustion, (2008).

[59] J.A. Miller, C.T. Bowman, Mechanism and modeling of nitrogen chemistry in combustion, Prog. Energy Combustion Sci. 15 (4) (1989) 287–338.
[60] S. Naha, A.M. Briones, S.K. Aggarwal, Effect of fuel blends on pollutant emissions in flames, (2004).
[61] C. Liu, F. Liu, J. Yang, Y. Mu, C. Hu, G. Xu, Experimental investigation of spray and combustion performances of a fuel-staged low emission combustor: effects of main swirl angle, J. Eng. Gas Turbines and Power. 139 (2017).
[62] J. Sangl, C. Mayer, T. Sattelmayer, Prediction of the NOx emissions of a swirl burner in partially and fully premixed mode on the basis of water channel laser induced fluorescence and particle image velocimetry measurements, J. Eng. Gas Turbines and Power. 136 (2014).
[63] L. Shi, Z. Fu, X. Duan, C. Cheng, Y. Shen, B. Liu, R. Wang, Influence of combustion system retrofit on NOx formation characteristics in a 300 MW tangentially fired furnace, Appl. Thermal Eng. 98 (2016) 766–777.
[64] S.R. Vatcha, Low-emission gas turbines using catalytic combustion, Energy Conversion and Management. 38 (1997) 1327–1334. doi: 10.1016/S0196-8904(96)00162-8.